

Optimizing Molecules using Efficient Queries from Property Evaluations

Samuel Hoffman¹, Vijil Chenthamarakshan¹, Kahini Wadhawan¹, Pin-Yu Chen^{1,*}, and Payel Das^{1,*}

¹IBM Research, Yorktown Heights, NY 10598, USA

*pin-yu.chen@ibm.com and daspa@us.ibm.com

ABSTRACT

Machine learning has shown potential for optimizing existing molecules with more desirable properties, a critical step towards accelerating new chemical discovery. In this work, we propose **QMO**, a generic query-based molecule optimization framework that exploits latent embeddings from a molecule autoencoder. QMO improves the desired properties of an input molecule based on efficient queries, guided by a set of molecular property predictions and evaluation metrics. We show that QMO outperforms existing methods in the benchmark tasks of optimizing molecules for drug likeliness and solubility under similarity constraints. We also demonstrate significant property improvement using QMO on two new and challenging tasks that are also important in real-world discovery problems: (i) optimizing existing SARS-CoV-2 Main Protease inhibitors toward higher binding affinity; and (ii) improving known antimicrobial peptides towards lower toxicity. Results from QMO show high consistency with external validations, suggesting effective means of facilitating molecule optimization problems with design constraints.

Introduction

Molecule optimization (MO) for improving the structural and/or functional profile of a molecule is an essential step in drug discovery and material design. Without further modeling or use of prior knowledge, the challenge of MO lies in the prohibitively large search space over all possible molecules. In recent years, machine learning has shown to be a promising tool for MO by combining domain knowledge and relevant datasets for efficient discovery¹⁻⁴. Compared to traditional high-throughput wet lab experiments or computer simulations that are time-consuming and expensive^{5,6}, machine learning can significantly accelerate MO by enabling quick turnover and instant feedback based on real-time model prediction and analysis⁷.

In particular, when drug discovery is needed at a pandemic speed for tackling urgent crisis, such as novel COVID-19 pandemic, a lot of attention has been directed to repurposing of existing drugs⁸. However, given the novel nature of the SARS-CoV-2 virus, the majority of existing drugs fail to show desired binding and inhibition of SARS-CoV-2 targets^{8,9}. Therefore, optimization of existing lead molecules toward better SARS-CoV-2 target binding affinity while keeping the molecular similarity high appears a promising first step for optimal drug design for COVID-19. Without loss of generality, we refer a lead molecule as the starting molecule to be optimized in order to meet a set of desired properties and constraints.

Many recent research studies that focus on machine learning enabled molecular optimization, represent a molecule as a string consisting of chemical units. For organic molecules, the SMILES representation¹⁰ is widely used, whereas for peptide sequences, a text string comprised of amino acid characters is a popular representation. Often, the optimization is performed on a learned representation space of the system of interest, which describes molecules as embedding vectors in a low-dimensional continuous space. A sequence-to-sequence encoder-decoder model, such as a (variational) autoencoder, can be used to learn continuous representations of the molecules in a latent space. Moreover, different optimization or sampling techniques based on the latent representation can be used to improve a molecule with external guidance from a set of molecular property predictors and simulators. The external guidance can be either explicitly obtained from physics-based simulations, (chem/bio-)informatics, wet-lab experiments, or implicitly learned from a chemical database.

Based on the methodology, the related works on machine learning for MO can be divided into two categories: *guided search* and *translation*. Guided search uses guidance from the predictive models and/or evaluations from statistical models, where the search can be either in the discrete molecule sequence space or through a continuous latent space (or distribution) learned by an encoder-decoder. Genetic algorithms^{11,12} and Bayesian optimization (BO)¹³ have been proposed for searching in the discrete sequence space, but their efficiency can be low in the case of high search dimension. Recent works have exploited latent representation learning and different optimization/sampling techniques for efficient search. Examples include the combined use of variational autoencoder (VAE) and BO¹⁴⁻¹⁷, VAE and sampling guided by a predictor^{18,19}, VAE and evolutionary algorithms²⁰, deep reinforcement learning and/or a generative network²¹⁻²⁵, and rejection sampling on an autoencoder²⁶. On

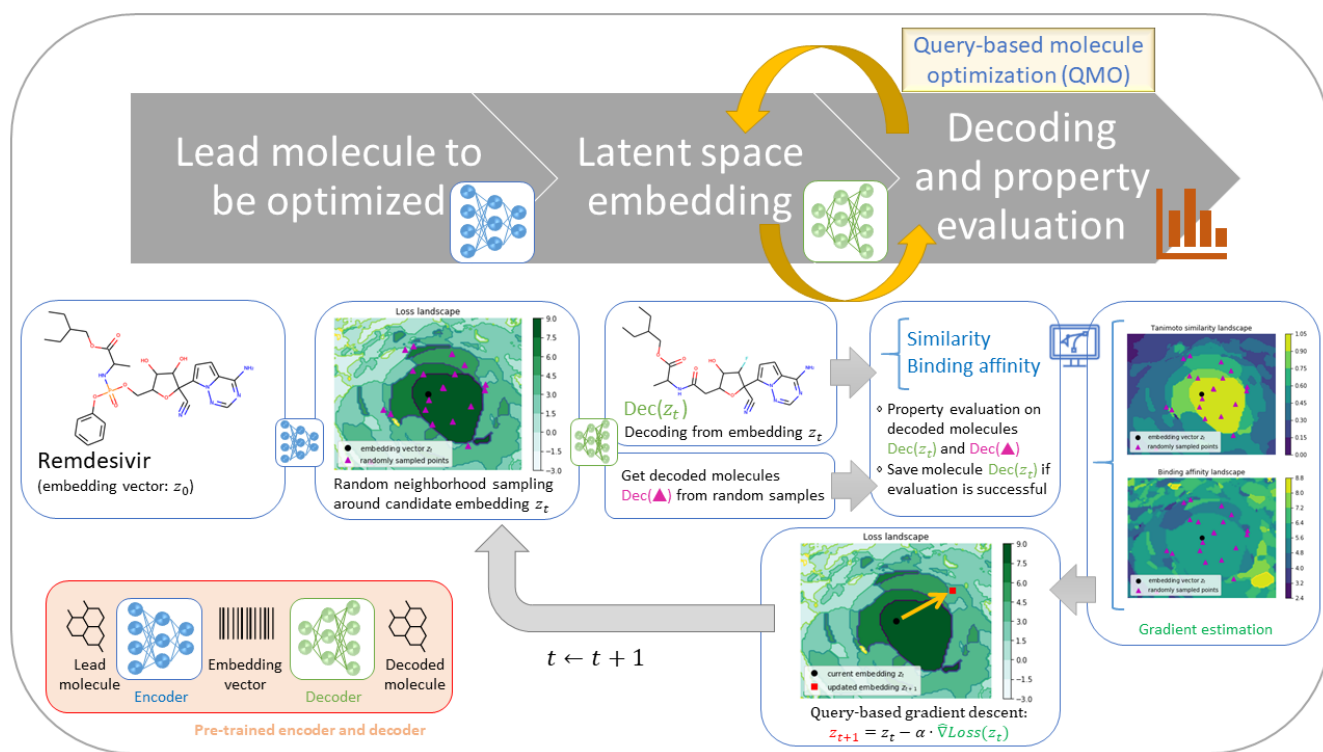


Figure 1. System illustration of the proposed query-based molecule optimization (QMO) framework. The QMO system progressively optimizes an input lead molecule (e.g., Remdesivir) according to a set of user-specified properties (e.g., binding affinity and Tanimoto similarity) by leveraging the learned molecule embeddings from a pair of pre-trained encoder and decoder (i.e. an autoencoder), and by evaluating the properties of the generated molecules. Given a candidate embedding z_t at the optimization step t , QMO randomly samples the neighboring vectors of z_t in the embedding space, evaluates the properties of the corresponding decoded molecules, and uses the evaluations for gradient estimation (see equation (4)) and queried-based gradient descent (see equation (3)) for finding the next candidate embedding vector z_{t+1} .

the other hand, translation-based approach treats molecule generation as a sequence-to-sequence translation problem^{27–30}. Examples of translation models are based on junction-tree^{31,32}, shape features¹⁵, hierarchical graph³³, and transfer learning³⁴. Comparing to guided search, translation-based approaches require the additional knowledge of paired sequences for learning to translate a lead molecule into an improved molecule. This knowledge may not be available for new MO tasks with limited information. For example, in the task of optimizing a set of known inhibitor molecules to better bind to SARS-Cov-2 target protein sequence while preserving the desired drug properties, a sufficient number of such paired molecule sequences is unavailable. We also note that these two categories are not exclusive. Guided search can be jointly used with translation.

In this paper, we propose a novel **Query-based Molecule Optimization (QMO)** framework, as illustrated in Figure 1. QMO uses an encoder-decoder and external guidance, but it differs from existing works in the following aspects: (i) QMO is a generic end-to-end optimization framework that reduces the problem complexity by decoupling representation learning and guided search. It applies to any *plug-in* (pre-trained) encoder-decoder with continuous latent representations. It also incorporates multiple predictions and evaluations made directly at the molecule sequence level into guided search without further model fitting. (ii) To achieve efficient end-to-end optimization with discrete molecule sequences and their continuous latent representations, QMO adopts a novel query-based guided search method based on zeroth order optimization^{35,36}, a technique that performs efficient mathematical optimization using only function evaluations (see Section 1 in the Supplementary Material for more details). Its query-based guided search enables direct optimization over the property evaluations provided by chemical informatics/simulation software packages or prediction APIs. To the best of our knowledge, this work is the first study that facilitates molecule optimization by disentangling molecule representation learning and guided search, and by exploiting zeroth order optimization for efficient search in the molecular property landscape.

We first demonstrate the effectiveness of QMO through two sets of standard benchmarks. On two existing and simpler MO benchmark tasks of optimizing³⁷, drug-likeness (QED)³⁸ and penalized logP (reflecting water solubility)¹⁸ with similarity constraints, QMO attains superior performance over existing baselines, showing at least 15% higher success on QED and 4.1

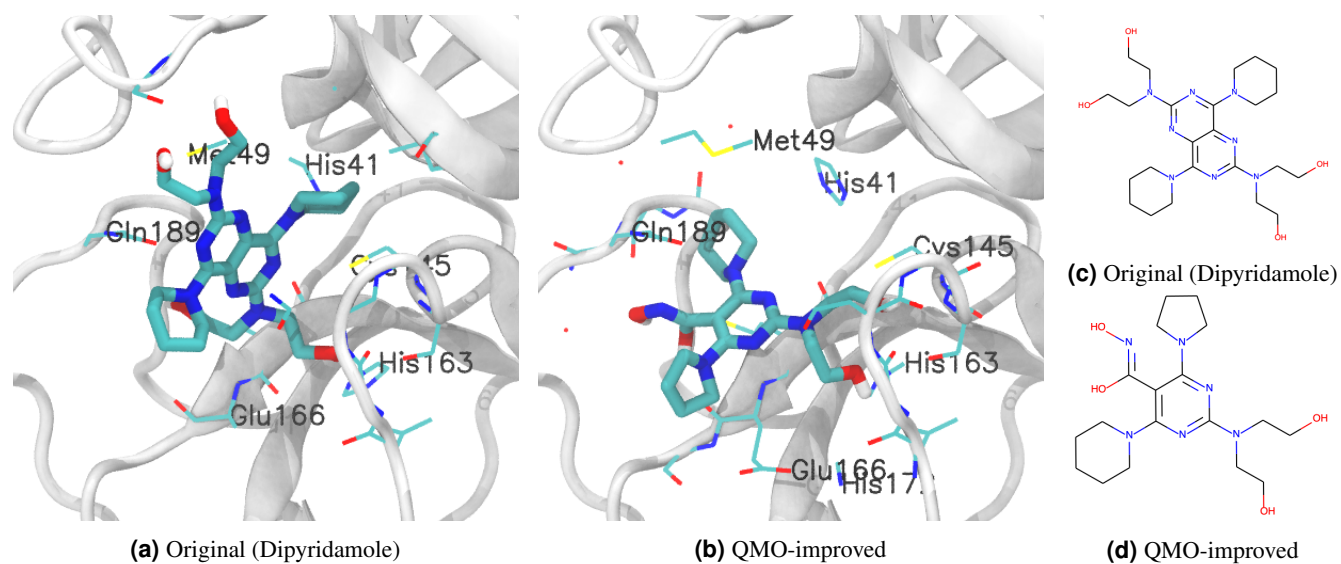


Figure 2. Top docking poses of Dipyridamole and its QMO-optimized variant with SARS-CoV-2 M^{Pro}, as obtained using AutoDock Vina. Their 2D structures are also shown. QMO optimizes the predicted affinity for the Dipyridamole variant from 4.43 to 8.02, while maintaining a Tanimoto similarity score of 0.79 and without changing the binding pocket significantly. MM/PBSA calculations for these poses show binding free energy improvement from -11.49 to -22.87 kcal/mol. Important residues from M^{Pro} substrate-binding pocket are also shown. See Table 3 for details.

better improvement on penalized logP.

Next, as a motivating discovery use-case that also, at least to some extent, reflect the complexity of real discovery problems³⁹, we demonstrate how QMO can be used to improve binding affinity of a number of existing inhibitor molecules to the SARS-CoV-2 Main Protease (M^{Pro}) sequence, one of the most extensively studied drug targets for SARS-CoV-2. As illustrated in Figure 2, we formulate this task as an optimization over predicted binding affinity (obtained using a pre-trained machine learning model) starting from an existing molecule of interest (i.e. a lead molecule). Since experimental IC₅₀ values are widely available, we use them ($\text{pIC}_{50} = -\log_{10}(\text{IC}_{50})$) as a measure for protein-ligand binding affinity. pIC_{50} of the optimized molecule is constrained to be above 7.5, a sign of good affinity, while the tanimoto similarity between the optimized and the original molecule is maximized. Retaining high similarity while optimizing the initial lead molecule means important chemical characteristics can be maximally preserved. Moreover, a high similarity to existing leads is important for rapid response to a novel pathogen such as SARS-CoV-2, as then it is more likely to leverage existing knowledge and manufacturing pipeline for synthesis and wet lab evaluation of the optimized variants. Moreover, the chance of optimized variants inducing adverse effects is potentially low. Our results show that QMO can find molecules with high similarity and improved affinity, while preserving other properties of interest such as drug-likeness.

We also consider the task of optimizing existing antimicrobial peptides toward lower selective toxicity, which is critical for accelerating safe antimicrobial discovery. In this task QMO shows high success rate ($\sim 72\%$) in improving the toxicity of antimicrobial peptides, and the properties of optimized molecules are consistent with external toxicity and antimicrobial activity classifiers. Finally, we perform property landscape visualization and trajectory analysis of QMO to illustrate its efficiency and diversity in finding improved molecules with desired properties.

Results

Representation of Molecules In our QMO framework, we model a molecule as a discrete string of chemical characters (i.e. a sequence). Depending on the downstream MO tasks, the sequence representation can either be a string of natural amino acids^{26,40}, or a string designed for encoding chemicals. In particular, the simplified molecular input line entry specification (SMILES) representation¹⁰ describes the structure of chemical species using short ASCII strings. Without loss of generality, we define $\mathbb{X}^m := \mathbb{X} \times \mathbb{X} \cdots \times \mathbb{X}$ as the product space containing every possible molecule sequence of length m , where \mathbb{X} denotes the set of all chemical characters. To elucidate the problem complexity, considering the 20 protein-building amino acids as characters in a peptide sequence, the number of possible candidates in the space of sequences with length $m = 60$ is already reaching the number of atoms in the known universe ($\sim 10^{80}$). Similarly, the space of small molecules with therapeutic potential is estimated to be on the order of $10^{6041,42}$. Therefore, the problem of MO in the ambient space \mathbb{X}^m can be computationally

inefficient as the search space grows combinatorially with the sequence length m .

Encoder-Decoder for Learning Latent Molecule Representations To address the issue of large search space for molecule sequences, QMO adopts an encoder-decoder framework. The encoder $\text{Enc} : \mathbb{X}^m \mapsto \mathbb{R}^d$ encodes a sequence $x \in \mathbb{X}^m$ to a low-dimensional continuous real-valued representation of dimension d , denoted by an embedding vector $z = \text{Enc}(x)$. The decoder $\text{Dec} : \mathbb{R}^d \mapsto \mathbb{X}^{m'}$ decodes the latent representation z of x back to the sequence representation, denoted by $\hat{x} = \text{Dec}(z)$. We note that depending on the encoder-decoder implementation, the input sequence x and the decoded sequence \hat{x} may be of different length. On the other hand, the latent dimension d is universal (fixed) to all sequences. In particular, Winter et al.⁴³ proposed a novel molecular descriptor and used it for an autoencoder to learn latent representations featuring high similarity between the original and the reconstructed sequences. QMO applies to any *plug-in* (pre-trained) encoder-decoder with continuous latent representations and thus decouples representation learning and guided search, in order to reduce the problem complexity of MO.

Molecule Optimization Formulation via Guided Search In addition to leveraging learned latent representations from a molecule encoder-decoder, our QMO framework incorporates molecular property prediction models and similarity metrics at the sequence level as external guidance. Specifically, for any given sequence $x \in \mathbb{X}^m$, we use a set of I separate prediction models $\{f_i(x)\}_{i=1}^I$ to evaluate the properties of interest for MO. In principle, for a candidate sequence x , a set of thresholds $\{\tau_i\}_{i=1}^I$ on its property predictions $\{f_i(x)\}_{i=1}^I$ is used for validating the condition $f_i(x) \geq \tau_i$ for all $i \in [I]$, where $[I]$ denotes the integer set $\{1, 2, \dots, I\}$. Moreover, we can simultaneously impose a set of J separate constraints $\{g_j(x|S) \geq \eta_j\}_{j=1}^J$ in the optimization process, such as molecular similarity, relative to a set of reference molecule sequences denoted by S .

Our QMO framework covers two practical cases in MO: (i) *optimizing molecular similarity while satisfying desired chemical properties* and (ii) *optimizing chemical properties with similarity constraints*. In what follows, we formally define our designed loss function of QMO for Case (i). Given a starting molecule sequence x_0 (i.e. a lead molecule) and a pre-trained encoder-decoder, let $x = \text{Dec}(z)$ denote a candidate sequence decoded from a latent representation $z \in \mathbb{R}^d$. Our QMO framework aims to find an optimized sequence by solving the following continuous optimization problem:

$$\text{Minimize}_{z \in \mathbb{R}^d} \underbrace{\sum_{i=1}^I \max\{\tau_i - f_i(\text{Dec}(z)), 0\}}_{\text{property validation loss (to be minimized)}} - \underbrace{\sum_{j=1}^J \lambda_j \cdot g_j(\text{Dec}(z)|S)}_{\text{molecular score (to be maximized)}} \quad (1)$$

The first term $\sum_{i=1}^I \max\{\tau_i - f_i(\text{Dec}(z)), 0\}$ quantifies the loss of property constraints and is presented as the sum of hinge loss over all property predictions, which approximates the binary property validation relative to the required thresholds $\{\tau_i\}_{i=1}^I$. It achieves the optimal value (i.e. 0) only when the candidate sequence $x = \text{Dec}(z)$ satisfies all the desired properties, which is equivalent to the condition that $f_i(\text{Dec}(z)) \geq \tau_i$ for all $i \in [I]$. The second term $\sum_{j=1}^J \lambda_j \cdot g_j(\text{Dec}(z)|S)$ corresponds to a set of molecular similarity scores to be maximized (therefore a minus sign in the minimization formulation). The reference sequence set S can be the starting sequence such that $S = \{x_0\}$, or a set of molecules. The positive coefficients $\{\lambda_j\}_{j=1}^J$ are associated with the set of molecular similarity scores $\{g_j(\text{Dec}(z)|S)\}_{j=1}^J$, respectively. It is worth mentioning that the use of the latent representation z as the optimization variable in a low-dimensional continuous space greatly facilitates the original MO problem in a high-dimensional discrete space. The optimization variable z can be initialized as the latent representation of x_0 , denoted by $z_0 = \text{Enc}(x_0)$.

Similarly, for Case (ii), the optimization problem is formulated as

$$\text{Minimize}_{z \in \mathbb{R}^d} \underbrace{\sum_{j=1}^J \max\{\eta_j - g_j(\text{Dec}(z)|S), 0\}}_{\text{molecular constraint loss (to be minimized)}} - \underbrace{\sum_{i=1}^I \gamma_i \cdot f_i(\text{Dec}(z))}_{\text{property score (to be maximized)}} \quad (2)$$

where $\{\eta_j\}_{j=1}^J$ are the similarity score constraints and $\{\gamma_i\}_{i=1}^I$ are positive coefficients of the property scores $\{f_i(\text{Dec}(z))\}_{i=1}^I$.

Query-based Molecule Optimization (QMO) Procedure Although we formulate MO as an unconstrained continuous minimization problem, we note that solving it for a feasible candidate sequence $x = \text{Dec}(z)$ is not straightforward because: (i) The output of the decoder $x = \text{Dec}(z)$ is a discrete sequence, which imposes challenges on any gradient-based (and high-order) optimization method since acquiring the gradient of z becomes non-trivial. Even resorting to the Gumbel-softmax sampling trick for discrete outputs⁴⁴, the large output space of the decoder may render it ineffective; (ii) In practice, many molecular property prediction models and molecular metrics are computed in an access-limited environment, such as prediction APIs and chemical softwares, which only allow inference on a queried sequence but prohibit other functionalities such as gradient computation. To address these two issues, we use zeroth order optimization in our QMO framework (see Methods section for

detailed procedure) to provide a generic and model-agnostic approach for solving the problem formulation in (1) and (2) using *only* inference results of $\{f_i\}_{i=1}^I$ and $\{g_j\}_{j=1}^J$ on queried sequences.

Let $\text{Loss}(z)$ denote the objective function to be minimized, as defined in either (1) or (2). Our QMO framework uses zeroth order gradient descent to find a solution, which mimics the descent steps on the loss landscape in gradient-based solvers but only uses the function values $\text{Loss}(\cdot)$ of queried sequences. Specifically, at the t -th iteration of the zeroth order optimization process, the iterate (candidate embedding vector) $z^{(t+1)}$ is updated by

$$z^{(t+1)} = z^{(t)} - \alpha_t \cdot \widehat{\nabla}_{\text{Loss}}(z^{(t)}), \quad (3)$$

where $\alpha_t \geq 0$ is the step size at the t -th iteration, and the true gradient $\nabla_{\text{Loss}}(z^{(t)})$ (which is challenging or infeasible to compute) is approximated by the pseudo gradient $\widehat{\nabla}_{\text{Loss}}(z^{(t)})$. The pseudo gradient $\widehat{\nabla}_{\text{Loss}}(z^{(t)})$ is estimated by Q independent random directional queries defined as

$$\widehat{\nabla}_{\text{Loss}}(z^{(t)}) = \frac{d}{\beta \cdot Q} \sum_{q=1}^Q [\text{Loss}(z^{(t)} + \beta u^{(q)}) - \text{Loss}(z^{(t)})] \cdot u^{(q)}, \quad (4)$$

where d is the dimension of the latent space of the encoder-decoder used in QMO, and $\beta > 0$ is a smoothing parameter used to perturb the embedding vector $z^{(t)}$ for neighborhood sampling with Q random directions $\{u^{(q)}\}_{q=1}^Q$ that are independently and identically sampled on a d -dimensional unit sphere. In our implementation, we sample $\{u^{(q)}\}_{q=1}^Q$ using a zero-mean d -dimensional isotropic Gaussian random vector divided by its Euclidean norm, such that the resulting samples are drawn uniformly from the unit sphere. Intuitively, the gradient estimator in (4) can be viewed as an average of Q random directional derivatives along the sampled directions $\{u^{(q)}\}_{q=1}^Q$. The constant $\frac{d}{\beta \cdot Q}$ in (4) ensures the norm of the estimated gradient is at the same order as that of the true gradient^{35,36}.

The QMO procedure is illustrated in Figure 1 with binding affinity and Tanimoto similarity as property evaluation criterion. Note that based on the iterative optimization step in (3), QMO only uses function values queried at the original and perturbed sequences for optimization. The query counts made on the Loss function for computing $\widehat{\nabla}_{\text{Loss}}(z^{(t)})$ is $Q + 1$ per iteration. Larger Q further reduces the gradient estimation error at the price of increased query complexity. When solving (1), an iterate $z^{(t)}$ is considered as a valid solution if its decoded sequence $\text{Dec}(z^{(t)})$ satisfies the property conditions $f_i(\text{Dec}(z^{(t)})) \geq \tau_i$ for all $i \in [I]$. Similarly, when solving (2), a valid solution $z^{(t)}$ means $g_j(\text{Dec}(z^{(t)}|S)) \geq \eta_j$ for all $j \in [J]$. Finally, QMO returns a set of found solutions (returning null if in vain). Detailed descriptions for the QMO procedure are given in Methods section.

Three Sets of Molecule Optimization Tasks with Multiple Property Evaluation Criterion In what follows, we demonstrate the performance of our proposed QMO framework on three sets of tasks that aim to optimize molecular properties with constraints, including standard MO benchmarks and challenging tasks relating to real-world discovery problems. The pre-trained encoder-decoder and the hyperparameters of QMO for each task are specified in Methods section.

Benchmarks on QED and Penalized logP Optimization We start with testing QMO on two single property targets: penalized logP and Quantitative Estimate of Druglikeness (QED)³⁸. LogP is the logarithm of the partition ratio of the solute between octanol and water. Penalized logP is defined as the logP minus the synthetic accessibility (SA) score¹⁸. Given a similarity constraint, finding an optimized molecule that maximizes drug-likeness of compounds using the QED score (ranging from 0 to 1)³⁸ or improves the penalized logP score¹⁸, are two widely used benchmarks. For a pair of original and optimized sequences (x_0, x) , we use the QMO formulation in (2) with the Tanimoto similarity (ranging from 0 to 1) over Morgan fingerprints⁴⁵ as $g_{\text{Tanimoto}}(x|x_0)$ and the interested property score (QED or penalized logP) as $f_{\text{score}}(x)$. Following the same setting as existing works, the threshold δ for $g_{\text{Tanimoto}}(x|x_0)$ is set as either 0.4 or 0.6. We use RDKit¹ to compute QED and logP, and use MOSES⁴⁶ to compute SA (synthetic accessibility), where $f_{\text{penalized logP}}(x) = \text{logP}(x) - \text{SA}(x)$.

In our experiments, we use the same set of 800 molecules with low penalized logP scores and 800 molecules with QED $\in [0.7, 0.8]$ chosen from the ZINC test set⁴⁷ as in Jin et al.¹⁸ as our starting sequences. We compare QMO with various guided-search and translation-based models in Tables 1 and 2. Baseline results are obtained from the literature^{31,34} that use machine learning for solving the same task.

For the QED optimization task, the success rate defined as the percentage of improved molecules having similarity greater than $\delta = 0.4$ is shown in Table 1. QMO outperforms all baselines by at least 15%. For penalized logP task, the molecules optimized by QMO outperform the baseline results by a significant margin, as shown in Table 2. The increased standard deviation in QMO is an artifact of having some molecules with much improved penalized logP scores (see Section 4 in the Supplementary Material).

¹RDKit: Open-source cheminformatics; <http://www.rdkit.org>

| Method | Success (%) |
|-------------------------|-------------|
| MMPA ²⁹ | 32.9 |
| JT-VAE ¹⁸ | 8.8 |
| GCPN ²⁴ | 9.4 |
| VSeq2Seq ³⁰ | 58.5 |
| VJTNN+GAN ³¹ | 60.6 |
| AtomG2G ³³ | 73.6 |
| HierG2G ³³ | 76.9 |
| DESMILES ³⁴ | 77.8 |
| QMO | 92.8 |

Table 1. Performance of drug likeness (QED) task with Tanimoto similarity constraint $\delta = 0.4$.

| Method | Improvement | |
|------------------------|-----------------------------------|-----------------------------------|
| | $\delta = 0.6$ | $\delta = 0.4$ |
| JT-VAE ¹⁸ | 0.28 ± 0.79 | 1.03 ± 1.39 |
| GCPN ²⁴ | 0.79 ± 0.63 | 2.49 ± 1.30 |
| VSeq2Seq ³⁰ | 2.33 ± 1.17 | 3.37 ± 1.75 |
| VJTNN ³¹ | 2.33 ± 1.24 | 3.55 ± 1.67 |
| QMO | 3.73 ± 2.85 | 7.71 ± 5.65 |

Table 2. Performance of penalized logP task at various Tanimoto similarity constraint value δ .

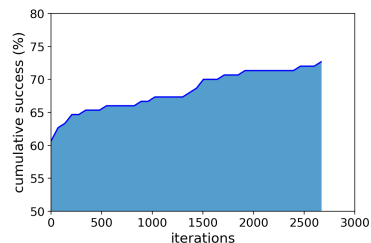


Figure 3. Cumulative success rate of AMP sequence optimization v.s. iterations using QMO.

Although the above-mentioned molecular property optimization tasks provide well-defined benchmarks for testing our QMO algorithm, it is well-recognized that such tasks are easy to solve and do not capture the complexity associated with real-world discovery³⁷. For example, it is trivial to achieve state-of-the-art results for logP optimization by generating long saturated hydrocarbon chains⁴⁸. Coley et al.³⁹ has proposed that molecular optimization goals that better reflect the complexity of real discovery tasks might include binding or selectivity attribute. Therefore, in the remaining of this paper, we consider two such tasks: (1) optimizing binding affinity of existing SARS-CoV-2 M^{Pro} inhibitor molecules and (2) lowering toxicity of known antimicrobial peptides.

Optimizing Existing Inhibitor Molecules and Applications to COVID-19 To provide a timely solution and accelerate the drug discovery against a new virus such as SARS-CoV-2, it is a sensible practice to optimize known leads to facilitate design and production as well as minimize the emergence of adverse effects. Here we focus on the task of optimizing the parent molecule structure of a set of existing SARS-CoV-2 M^{Pro} inhibitors. Specifically, we use the QMO formulation in (1), a pre-trained binding affinity predictor⁴⁹ f_{affinity} (output is pIC₅₀ value), and the Tanimoto similarity g_{Tanimoto} between the original and optimized molecules. Given a known inhibitor molecule x_0 , we aim to find an optimized molecule x such that $f_{\text{affinity}}(x) \geq \tau_{\text{affinity}}$ while $g_{\text{Tanimoto}}(x|x_0)$ is maximized.

For this task, we start by assembling 23 existing molecules shown to have weak to moderate affinity with SARS-CoV-2 M^{Pro}^{50,51}. These are generally in the μM range of IC₅₀, a measure of inhibitory potency (see Section 3 in the Supplementary Material for experimental IC₅₀ values). We choose the target affinity threshold τ_{affinity} as pIC₅₀ ≥ 7.5 , which implies strong affinity. The optimization results of each inhibitor are summarized in Table 3. Affinity predictions, Tanimoto similarity, quantitative estimation of drug-likeness (QED)³⁸, synthetic accessibility (SA)⁵², and the logarithm of partition coefficient (logP) properties are reported. The results show that predicted affinity is improved past the threshold for every starting compound while attaining similarity of 0.64 on average. QED is almost unchanged, on average, showing QMO preserves drug-likeness. SA increases only slightly, indicating synthesizability is still reasonable. Hydrophobicity (logP) decreases slightly meaning the molecules are more water-soluble.

Since all of these 23 inhibitors are reported to bind the substrate-binding pocket of M^{Pro}, we investigate possible binding mode alterations of the QMO-optimized molecules. It should be noted that, direct comparison of IC₅₀ with binding free energy is not always possible, as the relationship of binding affinity and IC₅₀ for a given compound varies depending on the assay conditions and the compound’s mechanism of inhibition⁵³. Further, high fidelity binding free energy estimation requires accounting for factors such as conformational entropy and explicit presence of the solvent. Nevertheless, we report binding free energy and mode for the QMO-optimized variants. For simplicity, we limit the analysis to achiral molecules. First, we run blind docking simulations using AutoDock Vina⁵⁴ over the entire structure of M^{Pro} with the exhaustiveness parameter set to 8. We further rescore top 3 docking poses for each of the original and QMO-optimized molecules using the Molecular Mechanics/Poisson Boltzmann Surface Area (MM/PBSA) method and AMBER forcefield⁵⁵, that is known to be more rigorous and accurate than the scoring function used in docking. Table 3 shows that variants of all 11 M^{Pro} inhibitors show better or comparable binding free energy, when compared to that of the original one. Next we inspect if any of the top-3 docking poses of the original as well as of QMO-optimized variants involves the substrate-binding pocket of M^{Pro}, as favorable interaction with that pocket is crucial for M^{Pro} function inhibition. As an illustration, Figure 2 shows top docking pose of Dipyridamole and its QMO-optimized variant to the M^{Pro} substrate-binding pocket. Consistent with more favorable MM/PBSA binding free energy, the QMO-optimized variant forms 11% more contacts (with a 5 Å distance cutoff between heavy atoms) with M^{Pro} substrate-binding pocket compared to Dipyridamole. Some of the M^{Pro} residues that explicitly form contacts with the

| compound | Affinity | | Similarity | QED | | SA | | logP | | BFE | |
|--------------------|----------|------|------------|-------|------|-------|------|-------|-------|-----------------|----------------|
| | orig. | imp. | | orig. | imp. | orig. | imp. | orig. | imp. | orig. | imp. |
| Dipyridamole | 3.94 | 7.84 | 0.65 | 0.31 | 0.22 | 2.99 | 2.99 | -0.02 | 0.55 | -11.49 (-21.39) | -22.87 |
| Favipiravir | 4.32 | 8.44 | 0.46 | 0.55 | 0.54 | 2.90 | 2.79 | -0.99 | -1.48 | -0.77 (-7.91) | -10.93 |
| Cinanserin | 4.43 | 8.02 | 0.79 | 0.44 | 0.22 | 2.07 | 2.41 | 4.38 | 1.73 | -11.51 (-15.61) | -11.92 |
| Tideglusib | 4.94 | 7.71 | 0.81 | 0.58 | 0.57 | 2.28 | 2.35 | 3.26 | 3.40 | ** | -13.31 |
| Bromhexine | 5.00 | 7.53 | 0.67 | 0.78 | 0.66 | 2.38 | 2.42 | 4.56 | 3.50 | -20.41 | -17.89 |
| PX-12 | 5.01 | 7.51 | 0.47 | 0.74 | 0.79 | 3.98 | 4.24 | 2.95 | 3.55 | * | * |
| Ebselen | 5.09 | 7.55 | 0.42 | 0.63 | 0.65 | 2.05 | 2.44 | 3.05 | 1.90 | -11.86 | -10.56 |
| Shikonin | 5.11 | 7.71 | 0.42 | 0.58 | 0.71 | 3.41 | 4.06 | 2.12 | 1.82 | * | * |
| Disulfiram | 5.54 | 7.51 | 0.57 | 0.57 | 0.36 | 3.12 | 3.66 | 3.62 | 5.37 | -20.43 | -9.81 (-17.98) |
| Entecavir | 5.55 | 7.68 | 0.39 | 0.53 | 0.40 | 4.09 | 4.78 | -0.83 | -1.29 | * | * |
| Hydroxychloroquine | 5.85 | 7.51 | 0.42 | 0.73 | 0.59 | 2.79 | 3.39 | 3.78 | 2.67 | * | * |
| Chloroquine | 6.07 | 7.58 | 0.66 | 0.76 | 0.79 | 2.67 | 2.69 | 4.81 | 4.30 | * | * |
| O6K | 6.18 | 7.70 | 0.62 | 0.25 | 0.71 | 4.12 | 3.56 | 2.22 | 0.75 | * | * |
| Remdesivir | 6.32 | 7.77 | 0.61 | 0.16 | 0.45 | 4.82 | 4.73 | 2.31 | 1.00 | * | * |
| Umifenovir | 6.36 | 7.60 | 0.73 | 0.38 | 0.42 | 2.68 | 2.63 | 5.18 | 5.12 | -16.08 | -20.87 |
| Lopinavir | 6.42 | 8.03 | 0.76 | 0.20 | 0.46 | 3.90 | 3.66 | 4.33 | 3.60 | * | * |
| Ambroxol | 6.46 | 7.97 | 0.64 | 0.71 | 0.75 | 2.50 | 3.22 | 3.19 | 2.17 | * | * |
| GS-441524 | 6.56 | 7.97 | 0.73 | 0.50 | 0.83 | 4.38 | 4.91 | -1.86 | 0.44 | * | * |
| Nelfinavir | 6.63 | 8.22 | 0.78 | 0.33 | 0.40 | 4.04 | 4.09 | 4.75 | 3.71 | * | * |
| Quercetin | 6.70 | 7.56 | 0.66 | 0.43 | 0.51 | 2.54 | 2.36 | 1.99 | 2.28 | -12.71 | -8.32 (-8.96) |
| N3 | 6.83 | 7.98 | 0.93 | 0.12 | 0.19 | 4.29 | 3.99 | 2.08 | 1.94 | * | * |
| Curcumin | 6.86 | 7.62 | 0.89 | 0.55 | 0.55 | 2.43 | 2.45 | 3.37 | 3.37 | -7.31 | -3.67 (-15.94) |
| Kaempferol | 6.90 | 7.72 | 0.67 | 0.55 | 0.64 | 2.37 | 2.36 | 2.28 | 3.23 | -11.86 | -13.48 |
| Average | 5.79 | 7.77 | 0.64 | 0.49 | 0.54 | 3.17 | 3.31 | 2.63 | 2.33 | | |

Table 3. Results for improving binding affinity of 23 existing SARS-CoV-2 M^{pro} inhibitor molecules. Original (orig.) and improved (imp.) values and their similarity are shown. The affinity threshold is set to ≥ 7.5 (pIC₅₀) while maximizing the Tanimoto similarity. Only the properties highlighted in blue are used in QMO. Relevant molecular properties — QED, SA, and logP — are also reported. The “BFE” column shows the binding free energy results obtained by MM/PBSA rescoring of the docking pose with M^{pro} substrate binding pocket (lower is better) using the webserver of Fast Amber Rescoring for PPI Inhibitors (<http://cadd.zju.edu.cn/farppi/>) with default forcefield (AMBER GAFF2 and ff14sb for ligand and protein, respectively) and parameter choices. More favorable BFE for alternative pocket is reported within parentheses. Chiral molecules (indicated with *) were excluded. Tideglusib was not possible to model with the webserver (**).

Dipyridamole variant are HIS172, ASP187, ARG188, and TYR54. Similar observations, e.g. higher number of contacts with M^{pro} substrate-binding pocket, which involves TYR54, were found for other exemplars of QMO variants, such as for Favipiravir and Umifenovir. See Section 4 in the Supplementary Material for extended blind docking analysis.

Optimization of Antimicrobial Peptides (AMPs) for Improved Toxicity As an additional motivating use-case, discovering new antibiotics at a rapid speed is critical to tackling the looming crisis of a global increase in antimicrobial resistance⁵⁶. AMPs are considered as promising candidates for next generation antibiotics. Optimal AMP design requires balancing between multiple, tightly interacting attribute objectives^{57,58}, such as high potency and low toxicity. As an attempt toward addressing this challenge, we show how QMO can be used to find improved variants of known AMPs with reported/predicted toxicity, such that the variants have lower predicted toxicity and high sequence similarity, when compared to original AMPs.

For the AMP optimization task, a peptide molecule is represented as a sequence of 20 natural amino acid characters. Using the QMO formulation in (1), subject to the constraints of toxicity prediction value (f_{tox}) and AMP prediction value (f_{AMP}), we aim to find most similar molecules for a set of toxic AMPs. The sequence similarity score (g_{sim}) to be maximized is computed using Biopython², which uses global alignment between two sequences (normalized by the length of the starting sequence) to evaluate the best concordance of their characters. See Methods section for detailed descriptions. The objective of QMO is to search for improved AMP sequences by maximizing similarity while satisfying AMP activity and toxicity predictions (i.e. classified as being AMP and non-toxic based on predictions from pre-trained deep learning models²⁶).

In our experiments, we use QMO to optimize 150 experimentally-verified toxic AMPs collected from public databases^{59,60} by Das et al.²⁶ as starting sequences. Note, the toxic annotation here does not depend on a specific type of toxicity, such as

²<http://www.biopython.org>.

| AMP and Toxicity Classifiers | Reported Accuracy (%) | Prediction Accuracy (%) on Starting Sequences | Prediction Rate (%) on QMO-optimized Sequences | Improvement (# of toxins (T) in starting sequences → # of non-toxins (NT) in optimized sequences) |
|---|-----------------------|---|--|---|
| AMP classifier ²⁶ used in QMO | 88.00 | 100 | 100 | – |
| iAMP-2L (AMP) ⁶³ | 92.23 | 91.74 | 72.47 | – |
| CAMP-RF (AMP) ⁶⁴ | 87.57 | 80.73 | 64.22 | – |
| Witten E.Coli (AMP) ⁶⁵ | 94.30 | 63.32 | 66.05 | – |
| Witten S.aureus (AMP) ⁶⁵ | 94.30 | 64.22 | 63.30 | – |
| Toxicity classifier ²⁶ used in QMO | 93.7 | 100 | 0 | 109 T → 109 NT |
| HLPpred-Fuse (toxicity) ⁶² | 97 | 61.46 | 44.03 | 67 T → 25 NT |
| HAPPENN (toxicity) ⁶¹ | 85.7 | 42.20 | 19.26 | 46 T → 31 NT |
| iAMP-2L + HAPPENN (AMP + Non-toxic) | – | 50.45 (AMP + Non-toxic) | 56.88 (AMP + Non-toxic) | 45 (AMP, T) → 22 (AMP, NT) |

Table 4. Reported accuracy, prediction rate, and property improvement for 109 pairs of starting and QMO-optimized sequences based on different AMP and Toxicity classifiers. The 109 starting sequences are experimentally verified toxic AMPs and are correctly predicted by the AMP and toxicity classifiers used in QMO. The external classifiers have varying prediction accuracy as they may yield incorrect predictions on some of starting sequences. The prediction rate on QMO-optimized sequences is defined as the fraction of AMP and/or toxin predictions. About 56.88% of QMO-optimized sequences are predicted as non-toxic AMPs by iAMP-2L + HAPPENN, showing high agreement with the classifiers used in QMO.

hemolytic toxicity. Figure 3 shows their cumulative success rate (turning toxic AMPs to non-toxic AMPs) using QMO up to the t -th iteration. Within the first few iterations, more than 60% molecules were successfully optimized. Eventually, about 72.66% (109/150) molecules can be successfully optimized. Table 5 shows some AMP sequences, and their property predictions and similarity scores. Figure 7 in the Supplementary Material depicts the optimization process of some AMP sequences. QMO can further improve similarity and maintain low predicted toxicity and high AMP values below the threshold after first success.

We perform additional validation of our optimization results by comparing QMO-improved sequences using a number of state-of-the-art AMP and toxicity predictors that are external classifiers not used in the QMO framework. Table 4 summarizes external classifiers’ prediction rates on 109 original and improved sequence pairs that are successfully optimized by QMO. We note that these external classifiers vary on training data size and type as well as on model architecture and report a range of accuracy. Data and models for the toxicity prediction problem are more rare, compared to those for the AMP classification problem. Further, external toxicity classifiers such as HAPPENN⁶¹ and HLPpred-fuse⁶² target explicitly predicting hemolytic toxicity. For these reasons, the predictions of the external classifiers on the original lead sequences may vary, when compared to ground-truth labels (see the third column in Table 4). Nonetheless, predictions on the QMO-improved sequences using external classifiers show high consistency in terms of toxicity improvement, when compared with the predictors used in QMO. Specifically, the predictions from iAMP-2L⁶³ and HAPPENN⁶¹ (hemolytic toxicity prediction) show that 56.88% (62/109) QMO-optimized molecules are predicted as non-toxic AMPs. Table 5 shows some examples of starting and improved AMP sequences as well as their sequence alignments and similarity scores.

Property Landscape Visualization and Trajectory Analysis To gain better understanding of how QMO optimizes a lead molecule with respect to the property constraints and objectives, we provide visual illustration of the property landscapes and search trajectories via QMO using a two-dimensional local interpolation on the molecule embedding space. Specifically, given the original embedding z_0 and the embedding of the best candidate z^* returned by QMO, we perform local grid sampling following two selected directions v_x and v_y , and then evaluate the properties of the decoded sequences from the sampled embeddings for property landscape analysis. For the purpose of visualizing the property landscape in low dimensions, we project the high-dimensional search trajectories $\{z_t\}_{t=1}^T$ to the two directions v_x and v_y . Figure 4 shows the landscape of Tanimoto similarity v.s. binding affinity prediction when using Remdesivir as the lead molecule, with the optimization objective of maximizing Tanimoto similarity while ensuring the predicted binding affinity is above a defined threshold 7.5. The two directions are the principal vector $z^* - z_0$ and a random vector orthogonal to the principal vector (see Methods section for more details). The trajectory shows how QMO leverages the evaluations of similarity and binding affinity for optimizing the lead molecule. Figure 4 also displays the common substructure of candidate molecules in comparison to the Remdesivir molecule in terms of subgraph similarity and their predicted properties over sampled iterations in QMO.

| Peptide Sequence (of amino acid symbols) original (top) – improved (bottom) sequence alignment | Toxicity, AMP (Yes/No) | | Similarity | |
|---|------------------------|------|------------|----------|
| | orig. | imp. | orig-orig | orig-imp |
| FFHHIFRGIVHVAKTIHRLVT--G FFHHVHVGVAAHAHTIHRVTVVVT | Y,Y | N,Y | 38.49 | 20.70 |
| AKKVFKRLGIGAVLWVLTG AKKVFKRLGDAILVWVTTG | Y,Y | N,Y | 33.71 | 24.03 |
| WFHHIFRGIVHVGKTIHRLVTG WFHHIHSGVIHEGSTIHRQVTG | Y,Y | N,Y | 40.76 | 30.41 |
| FWGALAKGALKLIGSLFSSFSKKD FYGMLAMLALKL-GSVFSKFSKKD | Y,Y | N,Y | 38.07 | 22.02 |
| IGGIISFFK-RLF IGGISFFKRLF | Y,Y | N,Y | 24.14 | 17.70 |
| FLPILAGLAAKIVPKLFLATKKC FLPMLAGLAAVIAPAAFCAAACC | Y,Y | N,Y | 38.70 | 27.68 |

Table 5. External validation of toxicity performed with HAPPENN⁶¹ (Y=Toxin, N=Non-Toxin) and AMP activity with iAMP-2L⁶³ (Y=AMP, N=Non-AMP). Pairwise alignment between original and improved sequence is also shown. Color coding follows red=mismatch, blue=match, and black=gap.

In addition to demonstrating the efficiency in optimizing lead molecules, we also study the diversity of the optimized molecules by varying the random seed used in QMO for query-based guided search. Figure 5 shows three different sets of trajectory on the landscape of predicted binding affinity when using Remdesivir as the lead molecule (see Methods section for more details). The optimization objective is the same as that of Figure 4. The visualization suggests that the trajectories are distinct and the best candidate molecule in each trajectory is distant from each other in the embedding space, suggesting that QMO can find a diverse set of improved molecules with desired properties.

Discussion and Conclusion

In this paper we propose QMO, a query-based end-to-end molecule optimization framework that readily applies to any pre-trained molecule encoder-decoder with continuous latent molecule embeddings and any set of property predictions and evaluation metrics. It features efficient guided search with molecular property evaluations and constraints obtained using predictive models and cheminformatics softwares.

On the simpler benchmark tasks for optimizing drug-likeness and penalized logP scores with similarity constraints, QMO demonstrates superior performance over baseline results. We also apply QMO to improve the binding affinity of existing inhibitors of the SARS-CoV-2 Main Protease, and to improve the toxicity of antimicrobial peptides. The QMO-optimized variants of existing drug molecules show favorable binding free energy with SARS-CoV-2 Main Protease upon blind docking and MM/PBSA rescoring, whereas the QMO-optimized peptides are consistently predicted to be antimicrobial and non-toxic by external peptide property predictors. The property landscape analysis and low-dimensional visualization of the optimization trajectories provide insights on how QMO navigates in the property space to find a diverse set of improved molecules with the desired properties. Our results show strong evidence for QMO to serve as a novel and practical tool for molecule optimization and other process/product design problems as well to aid accelerating chemical discovery with constraints. Future work will include integrating multi-fidelity expert feedback into the QMO framework for human-AI collaborative molecule optimization.

Methods

Procedure Descriptions of the QMO Framework

- **Procedure Inputs:** Pre-trained encoder-decoder; Molecular property predictors $\{f_i\}_{i=1}^I$ and thresholds $\{\tau_i\}_{i=1}^I$; Molecular similarity metrics $\{g_j\}_{j=1}^J$ and thresholds $\{\eta_j\}_{j=1}^J$; Total search iteration T ; Step size $\{\alpha_t\}_{t=0}^{T-1}$; Starting lead molecule sequence x_0 ; Reference sequence set S ; LOSS function from (1) or (2)
- **Procedure Initialization:** $z^{(0)} = \text{Enc}(x_0)$; $\mathbb{Z}_{\text{solution}} \leftarrow \{\emptyset\}$
- Repeat the following steps for T times, starting from $T = 0$:

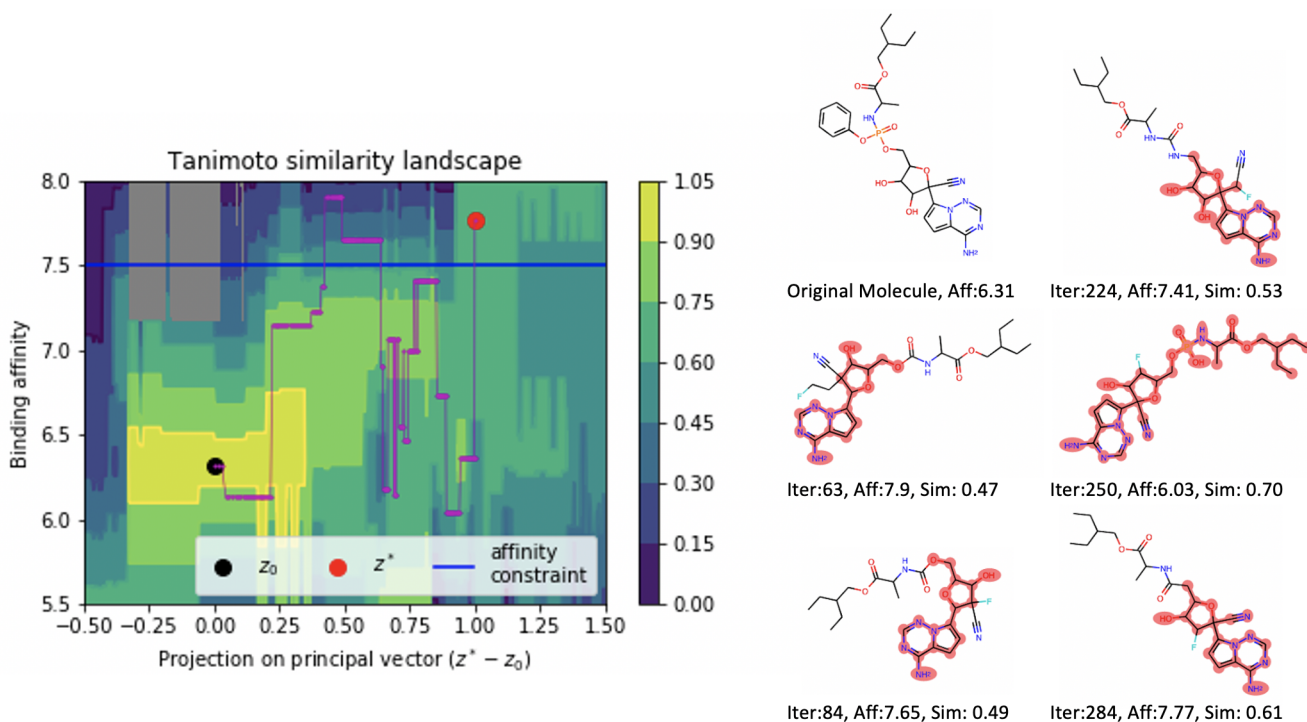


Figure 4. Left: QMO trajectory visualization on the landscape of Tanimoto similarity v.s. binding affinity prediction when using Remdesivir as the lead molecule. The optimization objective is to maximize Tanimoto similarity while ensuring the predicted binding affinity is above a defined threshold of 7.5. The gray area indicates infeasible region according to local grid search. Right: Common substructures over the QMO optimization process with respect to the Remdesivir structure and their property predictions. Iter denotes iteration index in QMO, Aff denotes affinity, and Sim denotes Tanimoto similarity. The highlighted part in red color indicates subgraph similarity.

- **Gradient Estimation:** Generate Q random unit-norm perturbations $\{u^{(q)}\}_{q=1}^Q$ and compute
$$\widehat{\nabla}_{\text{Loss}}(z^{(t)}) = \frac{d}{\beta \cdot Q} \sum_{q=1}^Q \left[\text{Loss}(z^{(t)} + \beta u^{(q)}) - \text{Loss}(z^{(t)}) \right] \cdot u^{(q)}$$
- **Pseudo Gradient Descent:** $z^{(t+1)} = z^{(t)} - \alpha_t \cdot \widehat{\nabla}_{\text{Loss}}(z^{(t)})$
- **Molecular property and constraint verification:** If solving for formulation (1), check $f_i(\text{Dec}(z^{(t)})) \geq \tau_i$ for all $i \in [I]$. If solving for formulation (2), check $g_j(\text{Dec}(z^{(t)})|S) \geq \eta_j$ for all $j \in [J]$.
- **Update valid molecule sequence:** $\mathbb{Z}_{\text{solution}} \leftarrow \mathbb{Z}_{\text{solution}} \cup \{z^{(t)}\}$

Procedure Convergence Guarantee and Implementation Details for QMO

Inherited from zero order optimization, QMO has algorithmic convergence guarantees. Under mild conditions on the true gradient (Lipschitz continuous and bounded gradient), the zeroth order gradient descent following (3) ensures QMO takes at most $O(\frac{d}{T})$ iterations to be sufficiently close to a local optimum in the loss landscape for a non-convex objective function^{35,36}, where T is the number of iterations. In addition to the standard zeroth order gradient descent method, our QMO algorithm can naturally adopt different zeroth order solvers, such as zeroth order stochastic and accelerated gradient descent.

In our QMO implementation, we use the zeroth-order version of the popular Adam optimizer⁶⁶ that automatically adjusts the step sizes $\{\alpha_t\}_{t=1}^{T-1}$ with an initial learning rate α_0 (see Section 2 in the Supplementary Material for more details). Empirically, we find that Adam performs better than stochastic gradient descent (SGD) in our tasks. The convergence of zeroth order Adam-type optimizer is given in⁶⁷. We will specify experimental settings, data descriptions, and QMO hyperparameters for each task. In all settings, QMO hyperparameters were tuned to a narrow range and then all the reported combinations were tried for each starting sequence. Among all feasible solutions returned by QMO, we report the one having the best molecular score given the required constraints. The stability analysis of QMO is studied in Section 5 of the Supplementary Material.

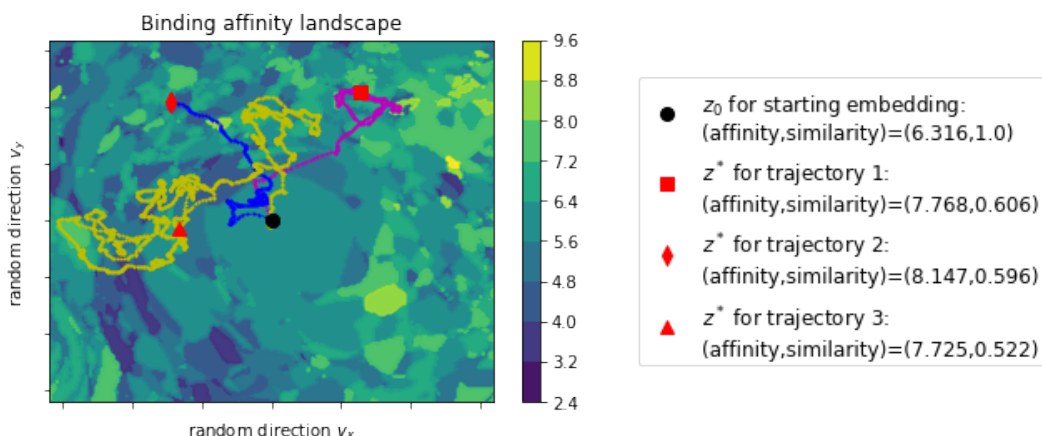


Figure 5. Three sets of QMO trajectory visualization on the landscape of predicted binding affinity when using Remdesivir as the lead molecule. The trajectory differs by the rand seed used in QMO for query-based guided search with random samples. The optimization objective is to maximize Tanimoto similarity while ensuring the predicted binding affinity is above a defined threshold 7.5. The visualization suggests that QMO can find a diverse set of improved molecules.

Experimental Settings

In our experiments, we run the QMO procedure based on the reported hyperparameter values and report the results of the best molecule found in the search process. The procedure will return null (that is, an unsuccessful search) if it fails to find a valid molecule sequence.

Benchmarks on QED and penalized logP The pre-trained encoder-decoder by Winter et al.⁴³ is used, with the latent dimension $d = 512$. For the penalized logP optimization task, we use $Q = 100$, $\beta = 10$, $\alpha_0 = 2.5$, $\gamma_{\text{penalized logP}} = 0.04$, and $T = 80$. For the QED task, we use $Q = 50$, $\beta = 10$, $\alpha_0 = 0.05$, $\gamma_{\text{QED}} = 4$, $T = 20$, and report the best results among 50 restarts. We find that for the QED task, using multiple restarts can further improve the performance (see Section 5 in the Supplementary Material for detailed discussion). For penalized logP, there is no reason to continue optimizing past 80 iterations as penalized logP can be increased almost arbitrarily without making the resulting molecule more useful for drug discovery²⁵ — even under similarity constraints, as we find. Therefore, we set $T = 80$ for the penalized logP task.

Optimizing Existing Inhibitor Molecules for SARS-CoV-2 Main Protease The pre-trained encoder-decoder by Winter et al.⁴³ is used, with the latent dimension $d = 512$. The hyperparameters of QMO are $Q = 10$, $T = 2000$, $\beta = \{10, 25\}$, $\alpha_0 = \{0.1, 0.05\}$, and $\lambda_{\text{Tanimoto}} = \{1, 10\}$.

Optimization of AMPs for Improved Toxicity The pre-trained predictors for toxicity and AMP by Das et al.²⁶ are used, with the latent dimension $d = 100$. The similarity between the original sequence x_0 and the improved sequence x is computed using the global alignment function in Biopython, formally defined as $g_{\text{sim}}(x|x_0) = \text{global-alignment}(x, x_0) / \log(\text{length}(x_0))$, where $\text{global-alignment}(x, x_0)$ is the value returned by the function `pairwise2.align.globalds(x, x_0, matlist.blosum62, -10, -1)` and $\log(\text{length}(x_0))$ is the log value of x_0 's sequence length. Blosum62 is the weight matrix for estimating alignment score⁶⁸, and $-10/-1$ is the penalty for opening/continuing a gap. The QMO parameters are $Q = 100$, $\beta = \{1, 10\}$, $\alpha_0 = \{0.1, 0.05, 0.01\}$, $\lambda_{\text{sim}} = 0.01$, and $T = 5000$. The toxicity property constraint is set as $f_{\text{tox}}(x) \leq 0.1529$ and amp as $f_{\text{amp}}(x) \geq 0.9998$. Binary classification on this threshold gives 93.7% accuracy for toxicity and 88.00% for AMP prediction on a large peptide database²⁶.

Trajectory Visualization

In Figure 4 and Figure 5, the optimization trajectory by QMO is visualized by projection on two selected directors v_x and v_y originated from the starting embedding z_0 . Specifically, in (4) we set $v_x = z^* - z_0$ and set v_y as a unit-norm randomly generated vector that is orthogonal to v_x . The two-dimensional local grid in the embedding space are then sampled according to $z_{\text{grid}}(x, y) = z_0 + x \cdot v_x + y \cdot \|z^*\|_2 \cdot u_y$, where $\|\cdot\|_2$ denotes the Euclidean distance and we sample x and y uniformly from $[-0.5, 1.5]$ and $[-2, 2]$, respectively. Note that by construction, $z_{\text{grid}}(0, 0) = z_0$ and $z_{\text{grid}}(1, 0) = z^*$. Then, we evaluate the Tanimoto similarity and binding affinity prediction of the grid and present their results in Figure 4. Similarly, in Figure 5 we set v_x and v_y to be two unit-norm randomly generated vectors, and set $z_{\text{grid}}(x, y) = z_0 + x \cdot \|z_0\|_2 \cdot v_x + y \cdot \|z_0\|_2 \cdot u_y$, where x and y are sampled uniformly from $[-1.6, 1.6]$.

References

1. Tkatchenko, A. Machine learning for chemical discovery. *Nat. Commun.* **11**, 1–4 (2020).
2. Townsend, J., Micucci, C. P., Hymel, J. H., Maroulas, V. & Vogiatzis, K. D. Representation of molecular structures with persistent homology for machine learning applications in chemistry. *Nat. communications* **11**, 1–9 (2020).
3. Méndez-Lucio, O., Baillif, B., Clevert, D.-A., Rouquié, D. & Wichard, J. De novo generation of hit-like molecules from gene expression signatures using artificial intelligence. *Nat. communications* **11**, 1–10 (2020).
4. Pesciullesi, G., Schwaller, P., Laino, T. & Reymond, J.-L. Transfer learning enables the molecular transformer to predict regio- and stereoselective reactions on carbohydrates. *Nat. Commun.* **11**, 1–8 (2020).
5. Polishchuk, P. G., Madzhidov, T. I. & Varnek, A. Estimation of the size of drug-like chemical space based on gdb-17 data. *J. computer-aided molecular design* **27**, 675–679 (2013).
6. Zhavoronkov, A. Artificial intelligence for drug discovery, biomarker development, and generation of novel chemistry (2018).
7. Ekins, S. *et al.* Exploiting machine learning for end-to-end drug discovery and development. *Nat. materials* **18**, 435 (2019).
8. Wu, C. *et al.* Analysis of therapeutic targets for sars-cov-2 and discovery of potential drugs by computational methods. *Acta Pharm. Sinica B* (2020).
9. Yang, J. *et al.* Molecular interaction and inhibition of sars-cov-2 binding to the ace2 receptor. *Nat. Commun.* **11** (2020).
10. Weininger, D. Smiles, a chemical language and information system. 1. introduction to methodology and encoding rules. *J. chemical information computer sciences* **28**, 31–36 (1988).
11. Reutlinger, M., Rodrigues, T., Schneider, P. & Schneider, G. Multi-objective molecular de novo design by adaptive fragment prioritization. *Angewandte Chemie Int. Ed.* **53**, 4244–4248 (2014).
12. Yuan, Y., Pei, J. & Lai, L. Ligbuilder 2: a practical de novo drug design approach. *J. chemical information modeling* **51**, 1083–1091 (2011).
13. Korovina, K. *et al.* Chembo: Bayesian optimization of small organic molecules with synthesizable recommendations. *arXiv preprint arXiv:1908.01425* (2019).
14. Gómez-Bombarelli, R. *et al.* Automatic chemical design using a data-driven continuous representation of molecules. *ACS central science* **4**, 268–276 (2018).
15. Skalic, M., Jiménez, J., Sabbadin, D. & De Fabritiis, G. Shape-based generative modeling for de novo drug design. *J. chemical information modeling* **59**, 1205–1214 (2019).
16. Griffiths, R.-R. & Hernández-Lobato, J. M. Constrained bayesian optimization for automatic chemical design using variational autoencoders. *Chem. Sci.* (2020).
17. Jiménez-Luna, J. *et al.* Deltadelta neural networks for lead optimization of small molecule potency. *Chem. Sci.* **10**, 10911–10918 (2019).
18. Jin, W., Barzilay, R. & Jaakkola, T. Junction tree variational autoencoder for molecular graph generation. *arXiv preprint arXiv:1802.04364* (2018).
19. Fu, T., Xiao, C. & Sun, J. Core: Automatic molecule optimization using copy & refine strategy. *AAAI Conf. on Artif. Intell.* (2020).
20. Winter, R. *et al.* Efficient multi-objective molecular optimization in a continuous latent space. *Chem. science* **10**, 8016–8024 (2019).
21. Olivecrona, M., Blaschke, T., Engkvist, O. & Chen, H. Molecular de-novo design through deep reinforcement learning. *J. cheminformatics* **9**, 48 (2017).
22. Guimaraes, G. L., Sanchez-Lengeling, B., Outeiral, C., Farias, P. L. C. & Aspuru-Guzik, A. Objective-reinforced generative adversarial networks (organ) for sequence generation models. *arXiv preprint arXiv:1705.10843* (2017).
23. Sanchez-Lengeling, B., Outeiral, C., Guimaraes, G. L. & Aspuru-Guzik, A. Optimizing distributions over molecular space. an objective-reinforced generative adversarial network for inverse-design chemistry (organic). *chemrxiv preprint chemrxiv.5309668* (2017).
24. You, J., Liu, B., Ying, Z., Pande, V. & Leskovec, J. Graph convolutional policy network for goal-directed molecular graph generation. In *Advances in neural information processing systems*, 6410–6421 (2018).

25. Zhou, Z., Kearnes, S., Li, L., Zare, R. N. & Riley, P. Optimization of molecules via deep reinforcement learning. *Sci. reports* **9**, 1–10 (2019).
26. Das, P. *et al.* Accelerating antimicrobial discovery with controllable deep generative models and molecular dynamics. *arXiv preprint arXiv:2005.11248* (2020).
27. Griffen, E., Leach, A. G., Robb, G. R. & Warner, D. J. Matched molecular pairs as a medicinal chemistry tool: miniperspective. *J. medicinal chemistry* **54**, 7739–7750 (2011).
28. Dossetter, A. G., Griffen, E. J. & Leach, A. G. Matched molecular pair analysis in drug discovery. *Drug Discov. Today* **18**, 724–731 (2013).
29. Dalke, A., Hert, J. & Kramer, C. mmpdb: An open-source matched molecular pair platform for large multiproperty data sets. *J. Chem. Inf. Model.* **58**, 902–910 (2018).
30. Bahdanau, D., Cho, K. & Bengio, Y. Neural machine translation by jointly learning to align and translate. In *International Conference on Learning Representations* (2015).
31. Jin, W., Yang, K., Barzilay, R. & Jaakkola, T. Learning multimodal graph-to-graph translation for molecule optimization. In *International Conference on Learning Representations* (2019).
32. Yang, K., Jin, W., Swanson, K., Barzilay, R. & Jaakkola, T. Improving molecular design by stochastic iterative target augmentation. *arXiv preprint arXiv:2002.04720* (2020).
33. Jin, W., Barzilay, R. & Jaakkola, T. Hierarchical graph-to-graph translation for molecules. *arXiv preprint arXiv:1907.11223* (2019).
34. Maragakis, P., Nisonoff, H., Cole, B. & Shaw, D. E. A deep-learning view of chemical space designed to facilitate drug discovery. *arXiv preprint arXiv:2002.02948* (2020).
35. Ghadimi, S. & Lan, G. Stochastic first-and zeroth-order methods for nonconvex stochastic programming. *SIAM J. on Optim.* **23**, 2341–2368 (2013).
36. Liu, S. *et al.* A primer on zeroth-order optimization in signal processing and machine learning. *IEEE Signal Process. Mag.* (2020).
37. Brown, N., Fiscato, M., Segler, M. H. & Vaucher, A. C. Guacamol: benchmarking models for de novo molecular design. *J. chemical information modeling* **59**, 1096–1108 (2019).
38. Bickerton, G. R., Paolini, G. V., Besnard, J., Muresan, S. & Hopkins, A. L. Quantifying the chemical beauty of drugs. *Nat. chemistry* **4**, 90–98 (2012).
39. Coley, C. W., Eyke, N. S. & Jensen, K. F. Autonomous discovery in the chemical sciences part ii: Outlook. *Angewandte Chemie Int. Ed.* (2019).
40. Qin, Z. *et al.* Artificial intelligence method to design and fold alpha-helical structural proteins from the primary amino acid sequence. *Extrem. Mech. Lett.* **36**, 100652 (2020).
41. Bohacek, R. S., McMartin, C. & Guida, W. C. The art and practice of structure-based drug design: a molecular modeling perspective. *Medicinal research reviews* **16**, 3–50 (1996).
42. Reymond, J.-L., Ruddigkeit, L., Blum, L. & van Deursen, R. The enumeration of chemical space. *Wiley Interdiscip. Rev. Comput. Mol. Sci.* **2**, 717–733 (2012).
43. Winter, R., Montanari, F., Noé, F. & Clevert, D.-A. Learning continuous and data-driven molecular descriptors by translating equivalent chemical representations. *Chem. science* **10**, 1692–1701 (2019).
44. Jang, E., Gu, S. & Poole, B. Categorical reparameterization with gumbel-softmax. In *International Conference on Learning Representations* (2017).
45. Rogers, D. & Hahn, M. Extended-connectivity fingerprints. *J. chemical information modeling* **50**, 742–754 (2010).
46. Polykovskiy, D. *et al.* Molecular Sets (MOSES): A Benchmarking Platform for Molecular Generation Models. *arXiv preprint arXiv:1811.12823* (2018).
47. Sterling, T. & Irwin, J. J. Zinc 15–ligand discovery for everyone. *J. chemical information modeling* **55**, 2324–2337 (2015).
48. Renz, P., Van Rompaey, D., Wegner, J. K., Hochreiter, S. & Klambauer, G. On failure modes in molecule generation and optimization. *Drug Discov. Today: Technol.* DOI: <https://doi.org/10.1016/j.ddtec.2020.09.003> (2020).
49. Chenthamarakshan, V. *et al.* Target-specific and selective drug design for covid-19 using deep generative models. *arXiv preprint arXiv:2004.01215* (2020).

50. Jin, Z. *et al.* Structure of mpro from sars-cov-2 and discovery of its inhibitors. *Nature* DOI: [10.1038/s41586-020-2223-y](https://doi.org/10.1038/s41586-020-2223-y) (2020).
51. Huynh, T., Wang, H. & Luan, B. In silico exploration of the molecular mechanism of clinically oriented drugs for possibly inhibiting sars-cov-2's main protease. *The J. Phys. Chem. Lett.* **0**, 4413–4420 (0).
52. Ertl, P. & Schuffenhauer, A. Estimation of synthetic accessibility score of drug-like molecules based on molecular complexity and fragment contributions. *J. Cheminformatics* **1**, 8 (2009).
53. Cournia, Z., Allen, B. & Sherman, W. Relative binding free energy calculations in drug discovery: recent advances and practical considerations. *J. chemical information modeling* **57**, 2911–2937 (2017).
54. Trott, O. & Olson, A. J. AutoDock Vina: improving the speed and accuracy of docking with a new scoring function, efficient optimization, and multithreading. *J. Comput. Chem.* **31**, 455–461 (2010).
55. Wang, Z. *et al.* farppi: a webserver for accurate prediction of protein-ligand binding structures for small-molecule ppi inhibitors by mm/pb (gb) sa methods. *Bioinformatics* **35**, 1777–1779 (2019).
56. Coates, A. R., Halls, G. & Hu, Y. Novel classes of antibiotics or more of the same? *Br. journal pharmacology* **163**, 184–194 (2011).
57. Tallorin, L. *et al.* Discovering de novo peptide substrates for enzymes using machine learning. *Nat. communications* **9**, 1–10 (2018).
58. Porto, W. F. *et al.* In silico optimization of a guava antimicrobial peptide enables combinatorial exploration for peptide design. *Nat. communications* **9**, 1–12 (2018).
59. Singh, S. *et al.* Satpdb: a database of structurally annotated therapeutic peptides. *Nucleic acids research* (2015).
60. Pirtskhalava, M. *et al.* Dbaasp v. 2: an enhanced database of structure and antimicrobial/cytotoxic activity of natural and synthetic peptides. *Nucleic acids research* **44**, D1104–D1112 (2016).
61. Timmons, P. B. & Hewage, C. M. Happenn is a novel tool for hemolytic activity prediction for therapeutic peptides which employs neural networks. *Sci. reports* **10**, 1–18 (2020).
62. Hasan, M. M. *et al.* HLPpred-Fuse: improved and robust prediction of hemolytic peptide and its activity by fusing multiple feature representation. *Bioinformatics* **36**, 3350–3356, DOI: [10.1093/bioinformatics/btaa160](https://doi.org/10.1093/bioinformatics/btaa160) (2020). <https://academic.oup.com/bioinformatics/article-pdf/36/11/3350/33329147/btaa160.pdf>.
63. Xiao, X., Wang, P., Lin, W.-Z., Jia, J.-H. & Chou, K.-C. iamp-2l: a two-level multi-label classifier for identifying antimicrobial peptides and their functional types. *Anal. biochemistry* **436**, 168–177 (2013).
64. Thomas, S., Karnik, S., Barai, R. S., Jayaraman, V. K. & Idicula-Thomas, S. Camp: a useful resource for research on antimicrobial peptides. *Nucleic acids research* **38**, D774–D780 (2010).
65. Witten, J. & Witten, Z. Deep learning regression model for antimicrobial peptide design. *bioRxiv* DOI: [10.1101/692681](https://doi.org/10.1101/692681) (2019). <https://www.biorxiv.org/content/early/2019/07/12/692681.full.pdf>.
66. Kingma, D. & Ba, J. Adam: A method for stochastic optimization. *Int. Conf. on Learn. Represent.* (2015).
67. Chen, X. *et al.* Zo-adamm: Zeroth-order adaptive momentum method for black-box optimization. In *Advances in Neural Information Processing Systems*, 7202–7213 (2019).
68. Henikoff, S. & Henikoff, J. G. Amino acid substitution matrices from protein blocks. *Proc. Natl. Acad. Sci.* **89**, 10915–10919 (1992).
69. Chen, P.-Y., Zhang, H., Sharma, Y., Yi, J. & Hsieh, C.-J. ZOO: Zeroth order optimization based black-box attacks to deep neural networks without training substitute models. In *ACM Workshop on Artificial Intelligence and Security*, 15–26 (2017).
70. Jeon, S. *et al.* Identification of antiviral drug candidates against sars-cov-2 from fda-approved drugs. *Antimicrob. Agents Chemother.* DOI: [10.1128/AAC.00819-20](https://doi.org/10.1128/AAC.00819-20) (2020). <https://aac.asm.org/content/early/2020/04/28/AAC.00819-20.full.pdf>.

Author contributions statement

S. Hoffman and V. Chenthamarakshan contributed to the SARS-CoV-2, QED, and penalized logP optimization experiments. K. Wadhawan contributed to the AMP experiment. S. Hoffman and P. Das contributed to the docking simulations. P.-Y. Chen contributed to QMO methodology design and property landscape analysis. V. Chenthamarakshan contributed to common substructure analysis. All authors contributed to paper writing.

Materials and Correspondence

Please contact Dr. Pin-Yu Chen (pin-yu.chen@ibm.com) and Dr. Payel Das (daspa@us.ibm.com)

Supplementary Material

Appendix

1 Background on Zeroth Order Optimization

In contrast to first-order (i.e. gradient-based) optimization, zeroth-order (ZO) optimization uses function values evaluated at queried data points to approximate the gradient and perform gradient descent, which we call *pseudo gradient descent*³⁵. It has been widely used in machine learning tasks when the function values are observable, while the gradient and other higher-order information are either infeasible to obtain or difficult to compute. A recent appealing application of ZO optimization is on efficient generation of prediction-evasive adversarial examples from information-limited machine learning models, known as *black-box adversarial attacks*⁶⁹. For the purpose of evaluating practical robustness, the target model only provides model predictions (e.g., a prediction API) to an attacking algorithm and does not reveal other information.

A major benefit of ZO optimization is its adaptivity from gradient-based methods. Despite using gradient estimates, many ZO optimization algorithms enjoy the same iteration complexity to converge to a stationary solution as their first-order counterparts under similar conditions. However, an additional multiplicative cost in a polynomial order of the problem dimension d (usually $O(d)$ or $O(\sqrt{d})$) will appear in the rate of convergence, due to the nature of query-driven pseudo gradient descent.

2 Additional Algorithm Descriptions

Algorithm 1 describes the zeroth order version of the Adam optimizer⁶⁶ used in our QMO implementation.

Algorithm 1 Query-based Molecule Optimization — Adam Variant (QMO-Adam)

- 1: **Input:** Trained Encoder-Decoder; Molecular property predictors $\{f_i\}_{i=1}^I$ and thresholds $\{\tau_i\}_{i=1}^I$; Molecular similarity metrics $\{g_j\}_{j=1}^J$ and thresholds $\{\eta_j\}_{j=1}^J$; Total search iteration T ; Initial step size α_0 ; Starting molecule sequence x_0 ; Reference sequence set S ; LOSS function
 - 2: **Initialization:** $z^{(0)} = \text{Enc}(x_0)$; $\mathbb{Z}_{\text{solution}} \leftarrow \{\emptyset\}$; $m^{(0)}, v^{(0)} \leftarrow 0$; $B_1 \leftarrow 0.9$; $B_2 \leftarrow 0.999$
 - 3: **for** $t = 0, 1, \dots, T - 1$ **do**
 - 4: **Gradient estimation:** $\widehat{\nabla}_{\text{LOSS}}(z^{(t)}) = \frac{d}{\beta \cdot Q} \sum_{q=1}^Q [\text{LOSS}(z^{(t)} + \beta u^{(q)}) - \text{LOSS}(z^{(t)})] \cdot u^{(q)}$
 - 5: **Adam update:**
 - 6: $m^{(t+1)} = B_1 \cdot m^{(t)} + (1 - B_1) \cdot \widehat{\nabla}_{\text{LOSS}}(z^{(t)})$
 - 7: $v^{(t+1)} = B_2 \cdot v^{(t)} + (1 - B_2) \cdot \widehat{\nabla}_{\text{LOSS}}(z^{(t)})^2$
 - 8: $\hat{m}^{(t+1)} = m^{(t+1)} / (1 - (B_1)^{t+1})$
 - 9: $\hat{v}^{(t+1)} = v^{(t+1)} / (1 - (B_2)^{t+1})$
 - 10: $z^{(t+1)} = z^{(t)} - \alpha_0 \cdot \frac{\hat{m}^{(t+1)}}{\sqrt{\hat{v}^{(t+1)} + \epsilon}}$
 - 11: **Molecular property and constraint verification:**
 - 12: **if** solving (1), check $f_i(\text{Dec}(z^{(t)})) \geq \tau_i$ for all $i \in [I]$ **then**
 - 13: **Save valid molecule sequence:** $\mathbb{Z}_{\text{solution}} \leftarrow \mathbb{Z}_{\text{solution}} \cup \{z^{(t)}\}$
 - 14: **if** solving (2), check $g_j(\text{Dec}(z^{(t)})|S) \geq \eta_j$ for all $j \in [J]$ **then**
 - 15: **Save valid molecule sequence:** $\mathbb{Z}_{\text{solution}} \leftarrow \mathbb{Z}_{\text{solution}} \cup \{z^{(t)}\}$
 - return** $\mathbb{Z}_{\text{solution}}$
-

3 More details on Model and Dataset

3.1 SARS-CoV-2 Use Case

In Table 6, we see experimental IC_{50} values for a few of the COVID-19 inhibitor candidates examined in Table 3 compared with their predicted affinity values. These are provided for reference.

Table 6. Experimental IC_{50} values copied from literature^{50,70} and converted to pIC_{50} for comparison. Affinity predictions are $pIC_{50} = -\log_{10}(IC_{50})$. The results show that the prediction is close to the experimental value.

| compound | Experimental | | Predicted pIC_{50} |
|-------------|-----------------------|------------|-------------------------|
| | IC_{50} (μM) | pIC_{50} | |
| Tideglusib | 1.55 | 5.81 | 4.94 |
| Chloroquine | 7.28 | 5.14 | 6.07 |
| Lopinavir | 9.12 | 5.04 | 6.42 |
| Disulfiram | 9.35 | 5.03 | 5.54 |
| Remdesivir | 11.41 | 4.94 | 6.32 |
| Shikonin | 15.75 | 4.80 | 5.11 |
| PX-12 | 21.39 | 4.67 | 5.01 |
| Cinanserin | 124.93 | 3.90 | 4.43 |

3.2 Antimicrobial Peptide Use Case

In our experiments, we used the labeled part of a large curated antimicrobial peptide (AMP) database in a recent AI-empowered antimicrobial discovery study²⁶. The AMP dataset has several attributes associated with peptides from which we used antimicrobial (AMP) and toxicity. The labeled dataset has only linear and monomeric sequences with no terminal modification and length up to 50 amino acids. The dataset contains 8683 AMP and 6536 non-AMP; and 3149 toxic and 16280 non-toxic sequences. For the starting AMP sequences, we consider sequences with up to length 15 and with property being both AMP and toxic. We then filter sequences for which our toxicity classifier predictions match with ground truth and obtain 167 sequences.

4 Additional Data Analysis and Visualization

4.1 Penalized log P Score Optimization

Figure 6 shows the distributions of improvement in penalized logP scores compared to the original molecules for the two similarity thresholds. The results show a long tail on the right-hand side, increasing the variance.

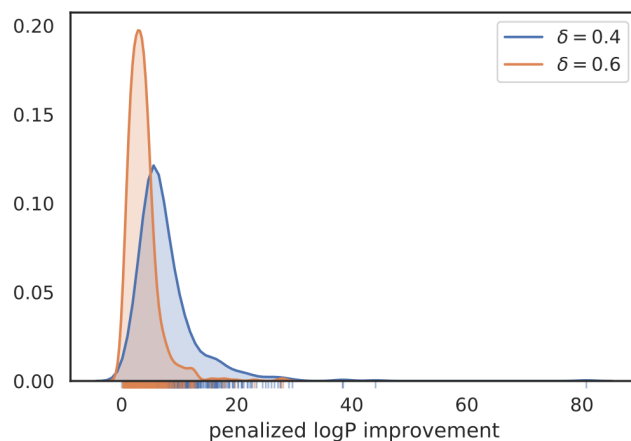


Figure 6. Distribution of improvement in penalized logP values after optimization by QMO on the 800 molecule set. A rug plot on the bottom shows the location of individual molecules for better visualization.

4.2 SARS-CoV-2 Use Case

Figure 7 shows the original and improved versions of all 23 COVID-19 inhibitor candidates. Table 8 shows the SMILES representations of these same molecules.

We also provide the extended results of docking analysis on the COVID-19 inhibitor candidates and their improved variants in Table 9. As noted in the paper, since there is no established one-to-one correlation between predicted pIC_{50} and binding free energy from docking, we use a binary (favorable/not favorable) threshold of -6 kcal/mol binding free energy. In addition, we investigate if the top binding modes revealed in docking do correspond to any of binding pockets reported in⁴⁹, which were estimated using PrankWeb³ and indexed by score. If the pocket does not change between original and improved molecules, we can expect a similar mode of inhibition of the target which is desirable (in the cases where we know the experimentally validated binding pocket of the original drug, e.g. see Figure 2).

³<http://prankweb.cz/>

Table 7. Results of QMO optimization of existing inhibitor molecules for COVID-19. For each pair of columns on either side of the dividing line, the left column shows the 2D structure of the original molecules and the right column shows the 2D structure of the QMO-optimized molecules which started from the initial state to the left with the original inhibitor name to the left of both.

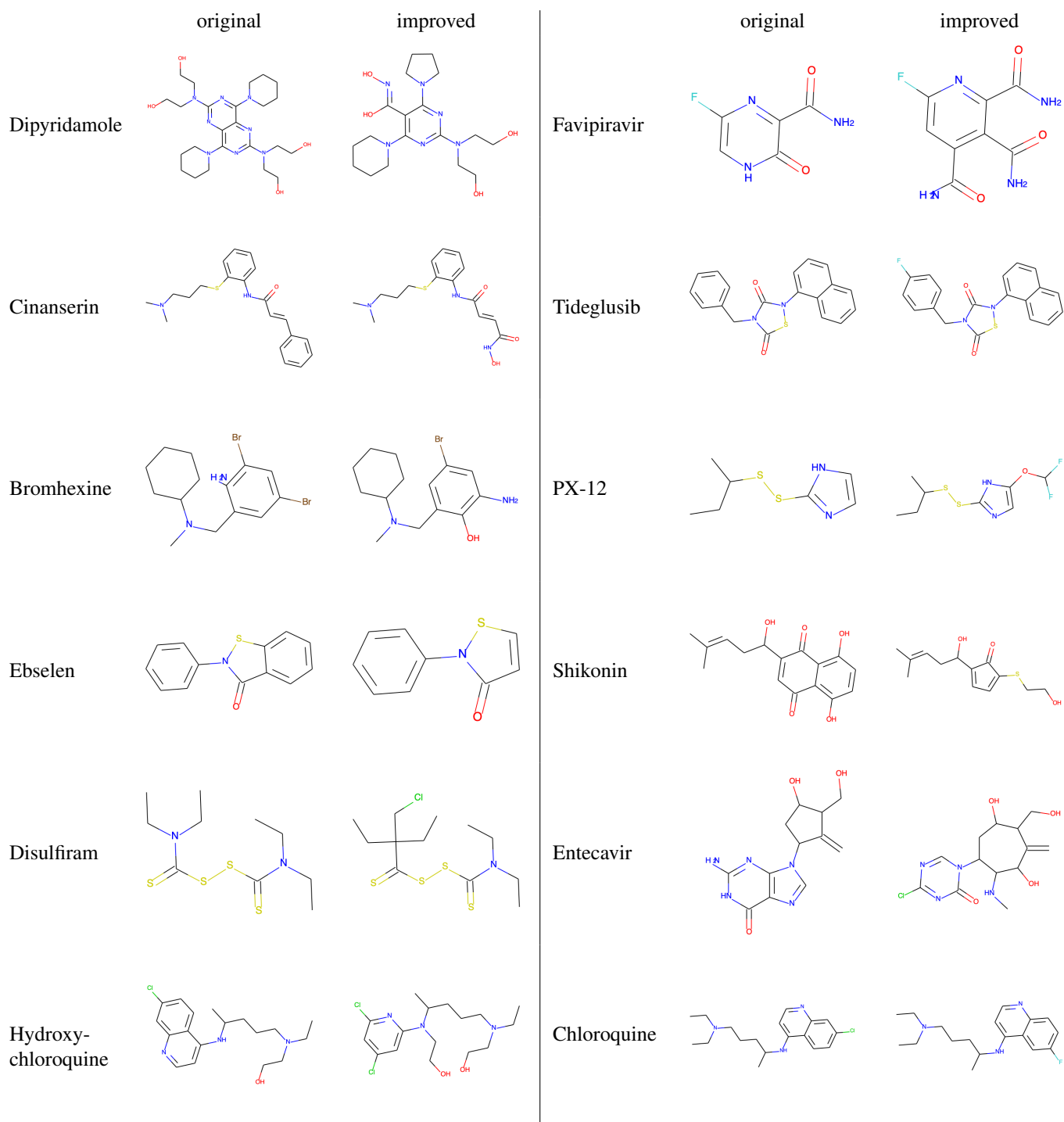
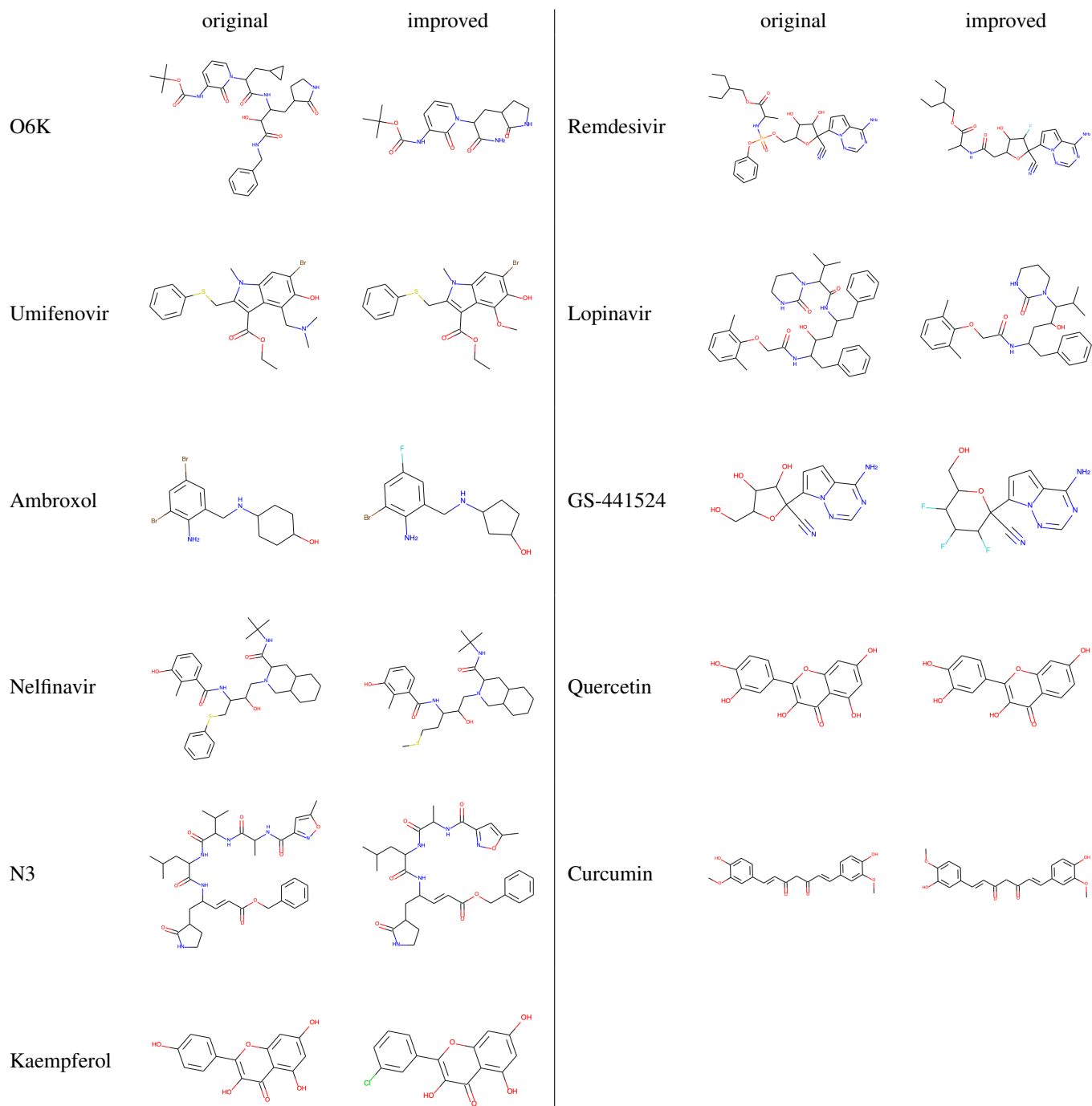


Table 7 continued



⁴The selenium atom in Ebselen is rare for drug molecules and cannot be handled by the encoder/decoder so it is substituted for sulfur before beginning optimization as in⁵⁰.

Table 8. SMILES representations of original and improved (QMO-optimized) inhibitor molecules.

| compound | | smiles |
|----------------------|----------|--|
| Dipyridamole | original | <chem>OCCN(CCO)c1nc(N2CCCCC2)c2nc(N(CCO)CCO)nc(N3CCCCC3)c2n1</chem> |
| | improved | <chem>OCCN(CCO)c1nc(N2CCCCC2)c(C(O)=NO)c(N2CCCCC2)n1</chem> |
| Favipiravir | original | <chem>NC(=O)c1nc(F)c[nH]c1=O</chem> |
| | improved | <chem>NC(=O)c1cc(F)nc(C(N)=O)c1C(N)=O</chem> |
| Cinanserin | original | <chem>CN(C)CCCSc1cccc1NC(=O)C=Cc1cccc1</chem> |
| | improved | <chem>CN(C)CCCSc1cccc1NC(=O)C=CC(=O)NO</chem> |
| Tideglusib | original | <chem>O=c1sn(-c2cccc3cccc23)c(=O)n1Cc1cccc1</chem> |
| | improved | <chem>O=c1sn(-c2cccc3cccc23)c(=O)n1Cc1ccc(F)cc1</chem> |
| Bromhexine | original | <chem>CN(Cc1cc(Br)cc(Br)c1N)C1CCCC1</chem> |
| | improved | <chem>CN(Cc1cc(Br)cc(N)c1O)C1CCCC1</chem> |
| PX-12 | original | <chem>CCC(C)SSc1ncc[nH]1</chem> |
| | improved | <chem>CCC(C)SSc1ncc(OC(F)F)[nH]1</chem> |
| Ebselen ⁴ | original | <chem>O=c1c2cccc2sn1-c1cccc1</chem> |
| | improved | <chem>O=c1ccsn1-c1cccc1</chem> |
| Shikonin | original | <chem>CC(C)=CCC(O)C1=CC(=O)c2c(O)ccc(O)c2C1=O</chem> |
| | improved | <chem>CC(C)=CCC(O)C1=CC=C(SCCO)C1=O</chem> |
| Disulfiram | original | <chem>CCN(CC)C(=S)SSC(=S)N(CC)CC</chem> |
| | improved | <chem>CCN(CC)C(=S)SSC(=S)C(CC)(CC)CC1</chem> |
| Entecavir | original | <chem>C=C1C(CO)C(O)CC1n1cnc2c(=O)[nH]c(N)nc21</chem> |
| | improved | <chem>C=C1C(O)C(NC)C(n2cnc(Cl)nc2=O)CC(O)C1CO</chem> |
| Hydroxychloroquine | original | <chem>CCN(CCO)CCCC(C)Nc1ccnc2cc(Cl)ccc12</chem> |
| | improved | <chem>CCN(CCO)CCCC(C)N(CCO)c1cc(Cl)cc(Cl)n1</chem> |
| Chloroquine | original | <chem>CCN(CC)CCCC(C)Nc1ccnc2cc(Cl)ccc12</chem> |
| | improved | <chem>CCN(CC)CCCC(C)Nc1ccnc2ccc(F)cc12</chem> |
| O6K | original | <chem>CC(C)(C)OC(=O)Nc1cccn(C(CC2CC2)C(=O)NC(CC2CCNC2=O)C(O)C(=O)NCc2cccc2)c1=O</chem> |
| | improved | <chem>CC(C)(C)OC(=O)Nc1cccn(C(CC2CCNC2=O)C(N)=O)c1=O</chem> |
| Remdesivir | original | <chem>CCC(CC)COC(=O)C(C)NP(=O)(OCC1OC(C#N)(c2ccc3c(N)nenn23)C(O)C1O)Oc1cccc1</chem> |
| | improved | <chem>CCC(CC)COC(=O)C(C)NC(=O)CC1OC(C#N)(c2ccc3c(N)nenn23)C(F)C1O</chem> |
| umifenovir | original | <chem>CCOC(=O)c1c(CSc2cccc2)n(C)c2cc(Br)c(O)c(CN(C)C)c12</chem> |
| | improved | <chem>CCOC(=O)c1c(CSc2cccc2)n(C)c2cc(Br)c(O)c(OC)c12</chem> |
| lopinavir | original | <chem>Cc1cccc(C)c1OCC(=O)NC(Cc1cccc1)C(O)CC(Cc1cccc1)NC(=O)C(C(C)C)N1CCNC1=O</chem> |
| | improved | <chem>Cc1cccc(C)c1OCC(=O)NC(Cc1cccc1)CC(O)C(C(C)C)N1CCNC1=O</chem> |
| Ambroxol | original | <chem>Nc1c(Br)cc(Br)cc1CNC1CCC(O)CC1</chem> |
| | improved | <chem>Nc1c(Br)cc(F)cc1CNC1CCC(O)C1</chem> |
| GS-441524 | original | <chem>N#CC1(c2ccc3c(N)ncnn23)OC(CO)C(O)C1O</chem> |
| | improved | <chem>N#CC1(c2ccc3c(N)ncnn23)OC(CO)C(F)C(F)C1F</chem> |
| Nelfinavir | original | <chem>Cc1c(O)cccc1C(=O)NC(CSc1cccc1)C(O)CN1CC2CCCCC2CC1C(=O)NC(C)(C)C</chem> |
| | improved | <chem>CSCCC(NC(=O)c1cccc(O)c1C)C(O)CN1CC2CCCCC2CC1C(=O)NC(C)(C)C</chem> |
| Quercetin | original | <chem>O=c1c(O)c(-c2ccc(O)c(O)c2)oc2cc(O)cc(O)c12</chem> |
| | improved | <chem>O=c1c(O)c(-c2ccc(O)c(O)c2)oc2cc(O)ccc12</chem> |
| N3 | original | <chem>Cc1cc(C(=O)NC(C)C(=O)NC(C(=O)NC(CC(C)C)C(=O)NC(C=CC(=O)OCc2cccc2)CC2CCNC2=O)C(C)C)no1</chem> |
| | improved | <chem>Cc1cc(C(=O)NC(C)C(=O)NC(CC(C)C)C(=O)NC(C=CC(=O)OCc2cccc2)CC2CCNC2=O)no1</chem> |
| Curcumin | original | <chem>COc1cc(C=CC(=O)CC(=O)C=Cc2ccc(O)c(OC)c2)ccc1O</chem> |
| | improved | <chem>COc1ccc(C=CC(=O)CC(=O)C=Cc2ccc(O)c(OC)c2)cc1O</chem> |
| Kaempferol | original | <chem>O=c1c(O)c(-c2ccc(O)cc2)oc2cc(O)cc(O)c12</chem> |
| | improved | <chem>O=c1c(O)c(-c2cccc(Cl)c2)oc2cc(O)cc(O)c12</chem> |

Table 9. Extended docking analysis: For each molecule, the top 3 docking poses (ranked by docking score) are shown with MM/PBSA binding free energy (kcal/mol) and corresponding binding pocket number. The best energy scores are highlighted: in red for the best energy that docks in pocket 1 or in blue if the lowest energy over the top 3 poses corresponds to a different pocket. Binding pockets are the same as identified in prior studies⁴⁹. As noted previously, Tideglusib (original) was not possible to model with AMBER forcefield (**).

| compound | Binding Free Energy | | | | | | Binding Pocket | | | | | |
|--------------|---------------------|---------------|---------------|---------------|---------------|---------------|----------------|---|---|-----------|---|---|
| | orig. pose | | | imp. pose | | | orig. pose | | | imp. pose | | |
| | 1 | 2 | 3 | 1 | 2 | 3 | 1 | 2 | 3 | 1 | 2 | 3 |
| Bromhexine | -11.89 | -14.01 | -20.41 | -13.86 | -15.72 | -17.89 | 1 | 0 | 0 | 1 | 1 | 0 |
| Cinanserin | -5.95 | -11.55 | -15.61 | -11.92 | -0.64 | -8.66 | 0 | 0 | 1 | 0 | 0 | 0 |
| Curcumin | -7.31 | -5.36 | -1.31 | -3.67 | -2.01 | -15.94 | 0 | 0 | 0 | 0 | 0 | 1 |
| Dipyridamole | -21.39 | -17.89 | -11.49 | -22.87 | -16.97 | -13.42 | 2 | 2 | 0 | 0 | 0 | 0 |
| Disulfiram | -20.39 | -20.43 | -19.73 | -17.98 | -9.81 | -9.99 | 0 | 0 | 0 | 1 | 0 | 1 |
| Ebselen | -11.16 | -11.69 | -11.86 | -10.56 | | | 1 | 0 | 0 | 0 | 2 | 3 |
| Favipiravir | -7.91 | -4.51 | -0.77 | -7.04 | -10.93 | -10.86 | 1 | 2 | 0 | 1 | 0 | 1 |
| Kaempferol | -7.42 | -11.86 | -11.18 | -13.48 | -6.52 | -11.45 | 1 | 0 | 0 | 0 | 0 | 0 |
| Quercetin | -12.71 | -9.68 | -10.08 | -8.32 | -8.96 | 9.25 | 0 | 0 | 0 | 0 | 3 | 0 |
| Tideglusib | ** | | | -13.31 | | | 0 | 1 | 0 | 0 | 0 | 1 |
| Umifenovir | -16.08 | -7.3 | -16.03 | -13.75 | -20.11 | -20.87 | 0 | 0 | 0 | 0 | 0 | 0 |

5 Stability Analysis of QMO

In this section, we selected two tasks to study the stability of QMO, in terms of run time comparison and the effect on the number Q of per-iteration random directions used in QMO.

5.1 QED Optimization

The total runtime for the QED task with $T = 20$ iterations and 50 random restarts was approximately 487 CPU/GPU hours or, spread over 32 cores, 15.2 hours of wall time. We complete 15 random restarts at a success rate of 85.9% in roughly 8 hours of wall time for 32 cores, the same time reported in²⁴. We ran all our experiments on machines with Intel Xeon E5-2600 CPUs and NVIDIA K80 GPUs.

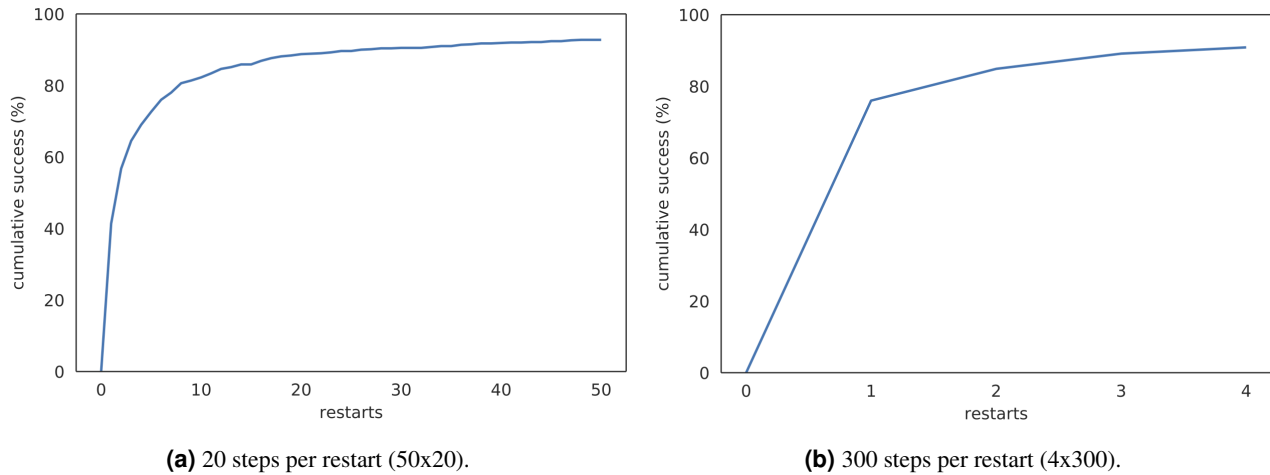


Figure 8. Cumulative success rate as a function of number of random restarts with 20 or 300 steps per restart for the QED task.

In examining the effect of multiple restarts, we show two configurations for running QMO on the QED task in Figure 8. Restarts happen if the algorithm is unable to find a successful candidate after the allotted number of steps. For this task, the algorithm stops after the first successful candidate is found. After 50 restarts at 20 steps (Figure 8a), we reach a success rate of 92.8% whereas after 4 restarts at 300 steps (Figure 8b), we only achieve 90.9% success despite taking about as long — 447 hours (4x300) compared to 487 hours (50x20). We conclude that for relatively easy tasks (single-constraint optimization) using a small number of steps T , restarting with a new random seed can be very effective since at early iterations the (effective) step size is relatively large and the guided search may tend to overshoot.

5.2 AMP Optimization

Figure 9 compares the effect of the per-iteration random direction sampling number Q in QMO on the cumulative success of the AMP experiments. We observe that setting larger Q value can improve the cumulative success rate but at the cost of increased number of property evaluations. The performance becomes similar once the Q value is sufficiently large, suggesting the stability of QMO.

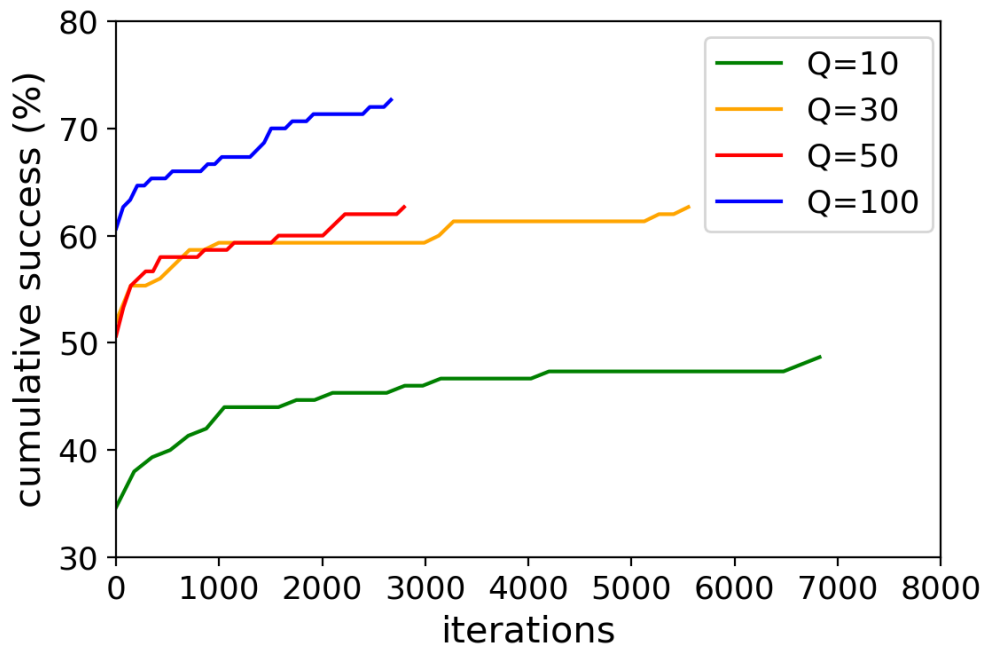


Figure 9. Cumulative success rate for the AMP task as a function of number of iterations with different per-iteration random sampling query value Q .